Inorg. Chem. **2004**, *43*, 5321–5334

Mixed-Ligand Organometallic Polymers Containing the "$Pd_2(dmb)_2^{2+}$" Fragment: Properties of the $\{Pd_2(dmb)_2(diphos)^{2+}\}_n$ Polymers/Oligomers in Solution and in the Solid State

Stéphanie Sicard,[1a] Jean-François Bérubé,[1a] Dalila Samar,[1a] Abdelhalim Messaoudi,[1a] Daniel Fortin,[1a] Frédéric Lebrun,[1a] Jean-François Fortin,[1a] Andreas Decken,[1b] and Pierre D. Harvey*,[1a]

Département de Chimie, Université de Sherbrooke, Sherbrooke, Quebec, Canada J1K 2R1, and Department of Chemistry, University of New Brunswick, Fredericton, New Brunswick, Canada E3B 6E2

Received January 18, 2004

The 1:1 reaction between the d^9–d^9 $Pd_2(dmb)_2Cl_2$ complex (dmb = 1,8-diisocyano-*p*-menthane) and the diphosphine ligands (diphos) bis(diphenylphosphino)butane (**5**, dppb), bis(diphenylphosphino)pentane (**6**, dpppen), bis-(diphenylphosphino)hexane (**7**, dpph), and bis(diphenylphosphino)acetylene (**8**, dpa) in the presence of $LiClO_4$ leads to the $\{[Pd_2(dmb)_2(diphos)](ClO_4)_2\}_n$ polymers. These new materials are characterized by NMR (^1H, ^{13}C, ^{31}P), IR, Raman, and UV–vis spectroscopies ($466 < \lambda_{max}(d\sigma–d\sigma^*) < 480$ nm), by ATG, XRD, and DSC methods, and by the capacity to make stand-alone films. From the measurements of the intrinsic viscosity in acetonitrile, the M_n ranges from 16000 to 18400 (12 to 16 units). The dinuclear model complex $[Pd_2(dmb)_2(PPh_3)_2](ClO_4)_2$ (**4**) is prepared and investigated as well. The molecular dynamic of the title polymers in acetonitrile solution is investigated by means of ^{13}C spin–lattice relaxation time (T_1) and nuclear Overhauser enhancement methods (NOE). The number of units determined by T_1/NOE methods is 3 to 4 times less than that found from the measurements of intrinsic viscosity, and is due to flexibility in the polymer backbone, even for bridging ligands containing only one (dmb) or two C–C single bonds (dpa). During the course of this study, the starting material $Pd_2(dmb)_2Cl_2$ was reinvestigated after evidence for oligomers in the MALDI-TOF spectrum was noticed. In solution, this d^9–d^9 species is a binuclear complex (T_1/NOE). This result suggests that the structure of the title polymers in solution and in the solid state may not be the same either. Finally, these polymers are strongly luminescent in PrCN glasses at 77 K, and the photophysical data (emission lifetimes, $1.50 < \tau_e < 2.75$ ns; quantum yields, $0.026 < \Phi_e < 0.17$) are presented. X-ray data for $[Pd_2(dppe)_2(dmb)_2](PF_6)_4$: monoclinic, space group *C*2/*c*, $a = 24.3735$ Å, $b = 21.8576$(13) Å, $c = 18.0034(9)$ Å, $b = 119.775(1)°$, $V = 8325.0(8)$ Å^3, $Z = 4$.

Introduction

The design of 1-D coordination polymers continues to be a very active field of research.[2] However, examples of polymers containing M_2-bonded fragments in the backbone are scarce.[3] Of relevant interest to this work, the chemistry of the dmb ligand was recently reviewed.[4] This bridging ligand exhibits a single C−C bond which leads to two conformers which are called U- and Z-forms (Chart 1), and the coordination products are overwhelmingly dominated by binuclear complexes.

Chart 1

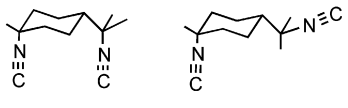

Polymers containing dmb also exist, but their occurrence in the literature is much less frequent, presumably due to the lack of X-ray characterization. The best examples are illustrated by the $\{M(dmb)_2^+\}_n$ and mixed-ligand polymers $\{M(dmb)(dppm)^+\}_n$ (dppm = bis(diphenylphosphino)-methane; Chart 2).[5]

This group also reported a series of examples of "polymers of M_2-bonded clusters" of the type $\{Pd_4(dmb)_4(dmb)^{2+}\}_n$ and

* To whom correspondence should be addressed. Tel: (819) 821-7092 or (819) 821-8000 ext 2005. Fax: (819) 821-8017. E-mail: P.Harvey@Usherbrooke.ca.

(1) (a) Université de Sherbrooke. (b) University of New Brunswick.

10.1021/ic049923b CCC: $27.50
Published on Web 07/17/2004

Chart 2

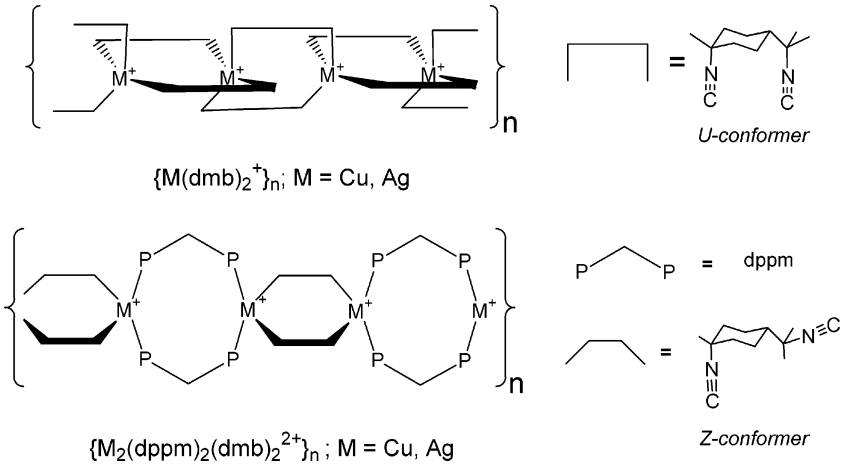

$\{Pt_4(dmb)_4(diphos)^{2+}\}_n$ (Chart 3), which were characterized by either crystallography or the measurements of the molecular weight (M_n) in solution.[6] These new materials contain unprecedented linear structures for 58-electron M_4 complexes of Pd and Pt. The optical, photophysical, and electric semi- and photoconductivity properties for these above singly and doubly bridged materials were also recently investigated.[7]

We now wish to report the syntheses and characterization of Pd_2-bonded organometallic polymers of the type $\{[Pd_2(dmb)_2(diphos)](ClO_4)_2\}_n$ with diphos = dppb, dpppen, dpph, and dpa. These polymers, which contain the $Pd_2(dmb)_2^{2+}$ fragment, are fully described in solution and in the solid state. During the course of this study, it became imperative that some properties of binuclear complexes such as $Pd_2(dmb)_2Cl_2$, $Pd_2(CN\text{-}t\text{-}Bu)_4Cl_2$, $Pd_2(dmb)_2(PPh_3)_2^{2+}$, and $Pd_2(dppe)_2(dmb)_2^{4+}$ and related reported polymers such as $\{Pd_2(diphos)_2(dmb)^{2+}\}_n$ (diphos = dppe, dppp, dppp**R**) be investigated in some detail. The molecular dynamics in solution have been addressed by T_1 and NOE measurements. The "$Pd_2(dmb)_2(P)_2^{2+}$" chromophore is also found to be strongly luminescent at 77 K (λ_e = 600 nm; $0.03 < \Phi_e < 0.17$) and is characterized by short emission lifetimes ($\tau_e = 1-3$ ns).

Chart 3

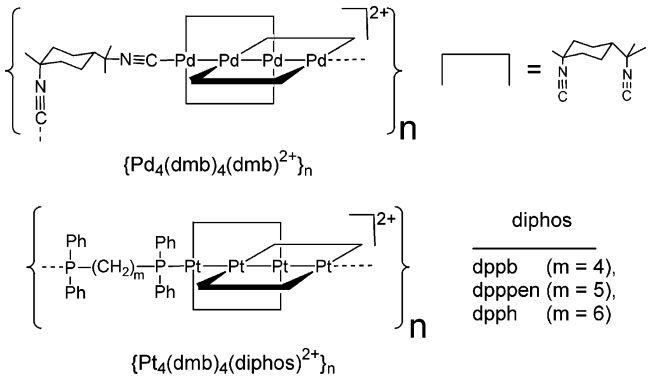

Experimental Section

Materials. $Pd_2(dmb)_2Cl_2$ (**1**),[8] $Pd_2(dmb)_2Cl_4$ (**2**),[8] $Pd_2(CN\text{-}t\text{-}Bu)_4Cl_2$ (**3**),[9] dmb,[10] and dpa[10] were synthesized according to procedures outlined in the literature. **1** and **2** were also synthesized using a

(2) For recent examples, see: (a) Schultheiss, N.; Powell, D. R.; Bosch, Eric *Inorg. Chem.* **2003**, *42*, 8886. (b) Gao, E.-Q.; Bai, S.-Q.; Wang, C.-F.; Yue, Y.-F.; Yan, C.-H. *Inorg. Chem.* **2003**, *42*, 8456. (c) Pradhan, R.; Desplanches, C.; Guionneau, P.; Sutter, J.-P. *Inorg. Chem.* **2003**, *42*, 6607. (d) Konar, S.; Zangrando, E.; Drew, M. G. B.; Mallah, T.; Ribas, J.; Chaudhuri, N. R. *Inorg. Chem.* **2003**, *42*, 5966. (e) Dong, Y.-B.; Cheng, J.-Y.; Huang, R.-Q.; Smith, M. D.; zur Loye, H.-C. *Inorg. Chem.* **2003**, *42*, 5699. (f) Sailaja, S.; Rajasekharan, M. V. *Inorg. Chem.* **2003**, *42*, 5675. (g) Li, G.; Hou, H.; Li, L.; Meng, X.; Fan, Y.; Zhu, Y. *Inorg. Chem.* **2003**, *42*, 4995. (h) Wan, Y.; Zhang, L.; Jin, L.; Gao, S.; Lu, S. *Inorg. Chem.* **2003**, *42*, 4985. (i) Barnett, S. A.; Blake, A. J.; Champness, N. R.; Wilson, C. *Dalton Trans.* **2003**, 2387. (j) Escuer, A.; Mautner, F. A.; Sanz, N.; Vicente, R. *Dalton Trans.* **2003**, 2121. (k) Khlobystov, A. N.; Brett, M. T.; Blake, A. J.; Champness, N. R.; Gill, P. M. W.; O'Neill, D. P.; Teat, S. J.; Wilson, C.; Schroeder, M. *J. Am. Chem. Soc.* **2003**, *125*, 6753. (l) Manson, J. L.; Gu, J.; Schlueter, J. A.; Wang, H.-H. *Inorg. Chem.* **2003**, *42*, 3950. (m) Hamilton, B. H.; Kelly, K. A.; Malasi, W.; Ziegler, C. J. *Inorg. Chem.* **2003**, *42*, 3067. (n) Hou, H.; Li, L.; Li, G.; Fan, Y.; Zhu, Y. *Inorg. Chem.* **2003**, *42*, 3501. (o) Tsao, T.-B.; Lee, G.-H.; Yeh, C.-Y.; Peng, S.-M. *Dalton Trans.* **2003**, 1465. (p) Konar, S.; Mukherjee, P. S.; Drew, M. G. B.; Ribas, J.; Chaudhuri, N. R. *Inorg. Chem.* **2003**, *42*, 2545. (q) Ciurtin, D. M.; Smith, M. D.; zur Loye, H.-C. *Dalton Trans.* **2003**, 1245. (r) Abrahams, B. F.; Batten, S. R.; Hoskins, B. F.; Robson, R. *Inorg. Chem.* **2003**, *42*, 2654. (s) He, Z.; He, C.; Gao, E.-Q.; Wang, Z.-M.; Yang, X.-F.; Liao, C.-S.; Yan, C.-H. *Inorg. Chem.* **2003**, *42*, 2206. (t) Konaka, H.; Wu, L. P.; Munakata, M.; Kuroda-Sowa, T.; Maekawa, M.; Suenaga, Y. *Inorg. Chem.* **2003**, *42*, 1928. (u) Song, J.-L.; Dong, Z.-C.; Zeng, H.-Y.; Zhou, W.-B.; Naka, T.; Wei, Q.; Mao, J.-G.; Guo, G.-C.; Huang, J.-S. *Inorg. Chem.* **2003**, *42*, 2136. (v) Seward, C.; Chan, J.; Song, D.; Wang, S. *Inorg. Chem.* **2003**, *42*, 1112. (w) Cui, Y.; Ngo, H. L.; White, P. S.; Lin, W. *Inorg. Chem.* **2003**, *42*, 652. (x) Meng, X.; Song, Y.; Hou, H.; Fan, Y.; Li, G.; Zhu, Y. *Inorg. Chem.* **2003**, *42*, 1306.

(3) (a) Tenhaeff, S. C.; Tyler, D. R. *Organometallics* **1991**, *10*, 473. (b) Tenhaeff, S. C.; Tyler, D. R. *J. Chem. Soc., Chem. Commun.* **1989**, 1459. (c) Tenhaeff, S. C.; Tyler, D. R. *Organometallics* **1992**, *11*, 1466. (d) Tenhaeff, S. C.; Tyler, D. R. *Organometallics* **1991**, *10*, 1116. (e) Male, J. L.; Lindsfors, B. E.; Covert, J.; Tyler, D. R. *Macromolecules* **1997**, *30*, 6404. (f) Nieckarz, G. F.; Tyler, D. R. *Inorg. Chim. Acta* **1996**, *242*, 303. (g) Male, J. L.; Yoon, M.; Glenn, A, G.; Weakly, T. J. R.; Tyler, D. R. *Macromolecules* **1999**, *32*, 3898. (h) Nieckarz, G. F.; Litty, J. J.; Tyler, D. R. *J. Organomet. Chem.* **1998**, *554*, 19.

(4) Harvey, P. D. *Coord. Chem. Rev.* **2001**, *219*, 17 and the references therein.

(5) (a) Perreault, D.; Drouin, M.; Michel, A.; Harvey, P. D. *Inorg. Chem.* **1992**, *31*, 3688. (b) Fortin, D.; Drouin, M.; Turcotte, M.; Harvey, P. D. *J. Am. Chem. Soc.* **1997**, *119*, 531. (c) Fortin, D.; Drouin, M.; Harvey, P. D. *J. Am. Chem. Soc.* **1998**, *120*, 5351. (d) Fournier, E.; Lebrun, F.; Decken, A.; Drouin, M.; Harvey, P. D. Submitted for publication. (e) Lebrun, F., M.Sc. Dissertation, Université de Sherbrooke, 2001.

(6) (a) Zhang, T.; M. Drouin, M.; Harvey, P. D. *Inorg. Chem.* **1999**, *38*, 1305. (b) Zhang, T.; Drouin, M.; Harvey, P. D. *Inorg. Chem.* **1999**, *38*, 957.

(7) Fortin, D.; Drouin, M.; Harvey, P. D. *Inorg. Chem.* **2000**, *39*, 2758.

modified procedure outlined below. The synthesis for [Pd(dppe)(CN-*t*-Bu)$_2$](PF$_6$)$_2$ will be published elsewhere.[11] The syntheses for the $\{[Pd_2(diphos')_2(dmb)](ClO_4)_2\}_n$ (diphos′ = dppe (**9**), dppp (**10**)) polymers are reported elsewhere.[12] PPh_3, CN-*t*-Bu, dppe, dppp, dppb, dpppen, dpph, and CD_3CN were purchased from Aldrich and were used as received. The solvents THF (Anachemia), acetonitrile (Fisher), acetone (Fisher), CH_2Cl_2 (ACP), pyridine (Aldrich), DMF (Aldrich), and diethyl ether (Aldrich) were purified according to literature procedures.[13] All reactions were carried out under an inert atmosphere (N_2 or argon) using Schlenck techniques, or inside a glovebox. ***CAUTION!*** *The handling of perchlorate salts of organometallic cations represents a potential explosive hazard. The use of small amounts is recommended.*

$Pd_2(dmb)_2Cl_4$ (2). To a 25 mL aqueous $PdCl_2$ solution (603 mg, 3.40 mmol) were added NaCl (608 mg, 10.4 mmol) and dmb (723 mg, 3.8 mmol). The mixture was stirred for 2 h, and a pale yellow solid precipitated. The crude solid was filtered and washed with water. The solid was dissolved in dichloromethane, dried over $MgSO_4$, and filtered. The solution was concentrated to dryness to give the desired compound. Yield: 76% (1.9 g). The sample data were checked against an authentic sample.[8]

$[Pd_2(dmb)_2Cl_2]$ (1). 2 (275 mg, 0.374 mmol), $Pd_2(dba)_3$ (342 mg, 0.374 mmol), and dmb (178 mg, 0.935 mmol) were dissolved in 50 mL of acetonitrile. The solution was stirred for 3 h under an inert atmosphere. The solution was concentrated to about 10 mL under vacuum. Diethyl ether (50 mL) was added to the solution, and a yellow precipitate appeared and was filtered. Yield: 84.5% (210 mg). The sample data were checked against an authentic sample.[8]

$[Pd_2(dmb)_2(PPh_3)_2](ClO_4)_2$ (4). 1 (45 mg, 0.068 mmol), $LiClO_4$ (18 mg, 0.17 mmol) and PPh_3 (35.5 mg, 0.135 mmol) were dissolved in 50 mL of water and 50 mL of dichloromethane. The solution was stirred for 2 h under an inert atmosphere. The residue was washed with water and extracted with dichloromethane. The organic layer was dried with $MgSO_4$, filtered, and concentrated to about 10 mL under vacuum. Diethyl ether (50 mL) was added to the solution, and a red precipitate appeared and was filtered. Yield: 30% (26 mg). ^{1}H NMR (CD_3CN): δ 7.70−7.15 (m, 30H, Ph), (m, 36H, dmb). ^{31}P {^{1}H} NMR (CD_3CN): δ 24.2. ^{13}C NMR (CD_3CN): δ 148.5, 142.2, 135.1, 134.8, 128.5, 65.2, 61.9, 44.9, 37.6, 28.2, 27.7, 22.4. IR (KBr) ν 2170 cm^{-1} (ν(C≡N)). Raman: ν 119 (ν(Pd$_2$)), 180 cm^{-1} (ν(PdP)). Anal. Calcd for $C_{60}H_{66}Cl_2N_4O_8P_2Pd_2$ (1316.88)·1H$_2$O·0.5acetonitrile: C, 54.72; H; 5.05; N, 4.25. Found: C, 54.05; H, 5.24; N, 4.21. The presence of H_2O and acetonitrile was confirmed by ^{1}H NMR and IR.

$\{[Pd_2(dmb)_2(dppb)](ClO_4)_2\}_n$ (5). This material was synthesized as outlined for **4**, except 1 equiv of dppb was used instead of PPh_3. Yield: 49% (41 mg). ^{1}H NMR (CD_3CN): δ 7.70−7.21 (m, 20H, Ph), 2.70 (m, 4H, CH_2P), 2.00 (m, 4H, CH_2), 1.70−0.96 (m, 36H, dmb). ^{31}P {^{1}H} NMR (CD_3CN): δ 25.6. ^{13}C NMR (CD_3CN): δ 148.5, 142.2, 135.1, 134.8, 128.5, 65.2, 61.9, 44.2, 37.6, 28.2, 27.8, 26.5, 25.6,24.9, 21.6, 22.4, 17.9. IR (KBr): ν 2164 cm^{-1} (ν(C≡N)). Raman (solid): ν 119 (ν(Pd$_2$)), 185 (ν(PdP)), 2172 (ν(C≡N)) cm^{-1}. Anal. Calcd for $C_{52}H_{64}Cl_2N_4O_8P_2Pd_2$ (1218.78)·0.2dppb: C, 53.05; H, 5.37; N, 4.29. Found: C, 52.79; H, 5.37; N, 4.32.

$\{[Pd_2(dmb)_2(dpppen)](ClO_4)_2\}_n$ (6). This material was synthesized as outlined for **4**, except 1 equiv of dpppen was used instead of PPh_3. Yield: 25%. ^{1}H NMR (CD_3CN): δ 7.70−7.15 (m, 20H, Ph), 2.70 (m, 4H, CH_2P), 2.15 (m, 6H, CH_2CH_2P), 2.01−1.05 (m, 36H, dmb). ^{31}P {^{1}H} NMR: 26.2. ^{13}C NMR (CD_3CN): δ 148.5, 142.2, 135.1, 134.8, 128.5, 65.2, 61.9, 44.9, 37.6, 28.2, 27.7, 25.6, 24.9, 23.8, 22.4, 21.6, 17.9. IR (KBr): ν 2162 (C≡N) cm^{-1}. Raman: ν 118 (ν(Pd)$_2$), 186 (ν(PdP)) cm^{-1}. Anal. Calcd for $C_{53}H_{66}Cl_2N_4O_8P_2Pd_2$ (1232.81). Anal. Calcd for $Pd_2C_{53}H_{66}N_4P_2O_8Cl_2Pd_2$·1.1H$_2$O·0.7CH$_3$CN: C, 50.99; H, 5.53; N, 5.14. Found: C, 51.00; H, 5.32; N, 5.18. The presence of H_2O and acetonitrile was confirmed by ^{1}H NMR and IR.

$\{[Pd_2(dmb)_2(dpph)](ClO_4)_2\}_n$ (7). This material was synthesized as outlined for **4**, except 0.5 equiv of dpph was used instead of PPh_3. Yield: 75%. ^{1}H NMR (CD_3CN): δ 7.70−7.15 (m, 20H, Ph), 2.80 (m, 4H,*CH*$_2$P), 2.25 (m, 8H, *CH*$_2$CH$_2$P), 2.04−0.96 (m, 36H, dmb). ^{31}P{^{1}H} NMR: δ 26.5. ^{13}C NMR (CD_3CN): δ 148.5, 142.2, 135.1, 134.8, 128.5, 65.2, 61.9, 44.9, 37.6, 28.2, 27.7, 25.6, 24.9, 23.8, 22.4, 21.6, 17.9. IR (KBr): 2158 (ν(N≡C)) cm^{-1}. Raman (solid): 119 (ν(Pd)$_2$), 184 (ν(PdP)), 2177 (ν(N≡C)) cm^{-1}. Chemical anal. Calcd for $Pd_2C_{54}H_{68}N_4P_2O_8Cl_2$ (1246.83): C, 52.02; H, 5.50; N, 4.49. Found: C, 51.63; H, 5.50; N, 4.69.

$\{[Pd_2(dmb)_2(dpa)](ClO_4)_2\}_n$ (8). This material was synthesized as outlined for **4**, except 0.5 equiv of dpa was used instead of PPh_3. Yield: 81%. ^{1}H NMR (CD_3CN): δ 7.64−7.57 (m, 8H, Ph), 7.35−7.32 (m, 12 H, Ph), 1.49−1.42 (m, 37 H, dmb). ^{31}P-{^{1}H} NMR: δ 23.5 (s). ^{13}C NMR (CD_3CN): δ 148.5, 142.2, 135.7, 135.1, 134.8, 132.8, 132.6, 132.5, 129.1, 128.7, 80.2, 65.2, 61.9, 44.9, 37.6, 28.2, 27.7, 25.6, 22.4. IR (KBr): ν 2167 (ν(N≡C)) cm^{-1}. Raman (solid): 120 (ν(Pd)$_2$), 181 (ν(PdP)). UV−vis (CH_3CN): 492 nm (27100 M^{-1} cm^{-1}). Anal. Calcd for $C_{50}H_{56}N_4P_2Pd_2Cl_2O_8$ (1186.70): C, 50.63; H, 4.72; N, 4.72. Found: C, 50.44; H, 4.57; N, 4.82.

1-Bromo-6-(2-naphthoxy)hexane (13). To solution of 2-naphthol (1.0 g, 6.90 mmol) in acetonitrile (6 mL) were added K_2CO_3 (2.0 g, 15.5 mmol) and 1,6-dibromohexane (6.40 mL, 41.4 mmol). The mixture was stirred at 50 °C under nitrogen for 15 h. The mixture was filtered and evaporated. The residue was dissolved in dichloromethane (100 mL). The solution was washed with water (100 mL), dried over Na_2SO_4, and evaporated. The residue was purified by column chromatography on silica gel in hexane−CH_2Cl_2 (90:10) to afford the white crystalline product **13** (1.276 g, 60%). ^{1}H NMR ($CDCl_3$): δ 7.78−7.71 (m, 3H, ar), 7.44 (t, J = 7.0, 1H, ar), 7.33 (t, J = 7.0, 1H ar), 7.17−7.13 (m, 2H, ar), 4.09 (t, J = 6.5, 2H, OCH_2), 3.44 (t, J = 6.8, 2H, CH_2Br), 1.90 (m, 4H, CH_2), 1.55 (m, 4H, CH_2). ^{13}C NMR ($CDCl_3$): δ 157.0, 134.6, 129.3, 128.9, 127.6, 126.3, 123.5, 118.9, 106.5, 67.7, 37.3, 33.8, 32.7, 29.1, 27.9, 25.4, 24.2. MS (EI): m/z = 306. Anal. Calcd for $C_{16}H_{19}OBr$ (307.23): C, 62.55; H, 6.23. Found: C, 62.50; H, 6.26. T_m: 36−38°C.

1,1-Bis(methoxycarbonyl)-7-(2-naphthoxy)heptane (14). NaH (0.593 g, 14.8 mmol) and KI (0.675 g, 4.07 mmol) were dissolved in 27 mL of 1:1 THF/DMF at 0°C. Then methyl malonate (1.84 mL, 16.1 mmol) was added. The mixture was stirred at room temperature, and **13** (4.11 g, 13.4 mmol) was added. The mixture was stirred overnight at 70°C under nitrogen. After the solution was allowed to cool to room temperature, it was diluted with diethyl

(8) Perreault, D.; Drouin, M.; Michel, A.; Harvey, P. D. *Inorg. Chem.*, **1992**, *31*, 2740.
(9) (a) Yamamoto, Y.; Yamazaki, H. *Bull. Chem. Soc. Jpn.* **1985**, *58*, 1843. (b) Otsuka, S.; Tatsumo, Y.; Ataka, K. *J. Am. Chem. Soc.* **1971**, *93*, 6705.
(10) For dmb, see: (a) Weber, W. D.; Gokel, G. W.; Ugi, I. K. *Angew. Chem., Int. Ed. Engl.* **1972**, *11*, 530. For dpa, see: (b) Walton, D. R. M.; Waugh, F. *J. Organomet. Chem.* **1972**, *37*, 45.
(11) Samar, D.; Fortin, J.-F.; Fortin, D.; Decken, A.; Harvey, P. D. To be submitted.
(12) Fournier, F.; Sicard, S.; Decken, A.; Harvey, P. D. *Inorg. Chem.* **2004**, *43*, 1491.
(13) (a) Perrin, D. D.; Armarego, W. L. F.; Perrin, D. R. *Purifications of laboratory chemicals*; Pergamon Press: Oxford, 1966. (b) Gordon, A. J.; Ford, R. A. *The chemist's companion, a handbook of practical data, techniques, and references*; Wiley: New York, 1972; p 436.

ether (50 mL) and washed with a solution of 1 N HCl (25 mL). The solution was washed with water and brine, dried over $MgSO_4$, and evaporated. The residue was purified by column chromatography on silica gel in ethyl acetate−petroleum ether (25:75) to afford the white crystalline product **14** (3.37 g, 70%). ^{1}H NMR (CD_2Cl_2): δ 7.77−7.71 (m, 3H, ar), 7.43 (t, J = 7.0, 1H, ar), 7.32 (t, J = 7.0, 1H, ar), 7.16−7.12 (m, 2H, ar), 4.06 (t, J = 6.5, 2H, OCH_2), 3.74 (s, 6H, CH_3), 3.38 (t, J = 7.5, 1H, CH), 1.86 (m, 4H, CH_2), 1.40 (m, 6H, CH_2). ^{13}C NMR ($CDCl_3$): δ 169.9, 157.0, 134.6, 129.3, 128.8, 127.6, 126.6, 126.2, 123.5, 118.9, 106.5, 67.8, 52.4, 51.6, 29.0, 28.7, 27.2, 25.8. IR (KBr): 1735 (ν(C═O)). MS (EI): m/z = 358. Anal. Calcd for $C_{21}H_{26}O_5$ (358.42): C, 70.37; H, 7.31. Found: C, 70.24; H, 7.40. T_m: 30−32°C.

2-(6-(2-Naphthoxy)hexyl)-1,3-dihydroxypropane (15). 14 (2.53 g, 7.07 mmol) was dissolved in 3 mL of diethyl ether. In another flask, $LiAlH_4$ (0.322 g, 8.48 mmol) was dissolved in 17 mL of diethyl ether and the solution was cooled to 0°C. The solution of **14** was added dropwise to the solution of $LiAlH_4$; 30 min after the addition, the mixture was stirred overnight at 70°C under nitrogen. Ethyl acetate was added dropwise until the precipitate changed color, from gray to white. HCl (1 N) was added until the solution was acidic. The solution was extracted with diethyl ether (40 mL) and washed with a solution 2% $NaHCO_3$ (30 mL) and with water (2 × 30 mL). The organic phase was dried over Na_2CO_3 and evaporated. The product was crystallized in diethyl ether at 0 °C to lead to compound **15** as a white solid (1.10 g, 51%). ^{1}H NMR ($CDCl_3$): δ 7.80−7.74 (m, 3H, ar), 7.46 (t, J = 7.0, 1H, ar), 7.35 (t, J = 7.0, 1H, ar), 7.20−7.14 (m, 2H, ar), 4.05 (t, J = 6.5, 2H, OCH_2), 3.75 (m, 4H, CH_2OH), 2.04 (br s, 2H, OH), 1.89−1.77 (m, 3H, CH and OCH_2CH_2), 1.54−1.26 (m, 8H, CH_2). ^{13}C NMR ($CDCl_3$): δ 156.8, 134.5, 129.2, 128.7, 127.5, 126.6, 126.2, 123.3, 118.8, 106.4, 67.7, 65.7, 41.8, 29.5, 29.1, 27.5, 27.0, 25.9. IR (KBr): 3292 (ν(OH)). MS (EI) m/z = 302. Anal. Calcd for $C_{19}H_{26}O_3$ (302.41): C, 75.46; H, 8.67. Found: C, 75.28; H, 8.84. T_m: 73−75°C.

2-(6-(2-Naphthoxy)hexyl)-1,3-di(toluene-4-sulfonyl)propane (16). 15 (0.281 g, 0.929 mmol) was dissolved in dichloromethane (10 mL), triethylamine (0.260 mL, 1.87 mmol) was added to the mixture, and the solution was cooled to 0°C. *p*-Toluenesulfonyl chloride (0.367 g, 1.93 mmol) was added, and the solution was stirred overnight at room temperature under nitrogen. The solvent was evaporated, and the residue was dissolved in dichloromethane (100 mL). The solution was washed with water, dried over Na_2SO_4, and evaporated. An oil was obtained, and the product was precipitated with methanol and filtered to lead to compound **16** as a white solid (0.361 g, 64%). ^{1}H NMR ($CDCl_3$): δ 7.78−7.10 (m, 15H, ar), 4.04 (t, J = 6.5, 2H, OCH_2), 3.92 (dd, 4H, CH_2OS), 2.44 (s, 3H, CH_3), 1.95 (sept, J = 5.5, 1H, CH), 1.76 (q J = 7, 2H, CH_2), 1.52−1.10 (m, 8H, CH_2). ^{13}C NMR ($CDCl_3$): δ 159.0, 154.4, 147.1, 136.5, 134.4, 131.8, 131.1, 130.7, 129.7, 129.4, 128.5, 128.2, 125.3, 120.8, 110.1, 108.3, 70.8, 69.8, 39.8, 31.0, 28.7, 28.1, 27.7, 23.3. IR (KBr): 1361 (ν(S═O)), 1185 (S═O). MS (EI): 610. Anal. Calcd for $C_{33}H_{38}O_7S_2$ (610.78): C, 64.89; H, 6.23; S, 10.50. Found: C, 64.85; H, 6.32; S, 10.29. T_m: 82−84 °C.

2-(6-(2-Naphthoxy)hexyl)-1,3-bis-diphenylphosphinopropane (17) (dpppR). 16 (0.298 g, 0.488 mmol) was dissolved in THF (10 mL) in the dark. In another flask, $KPPh_2$ (1.96 mL (solution 0.50 M in THF), 0.982 mmol) was dissolved in THF (30 mL). The solution of **16** was added dropwise to the $KPPh_2$ solution. The mixture was stirred overnight at room temperature; 5 mL of methanol was added, and the solution was stirred for 10 min. Pentane (30 mL) was added, and the solution was shaken vigorously and filtered. The product was crystallized in ether/methanol at 0 °C, to lead to the compound (**17**, dpppR) (oil, 0.21 g, 67%). ^{1}H NMR ($CDCl_3$): δ 7.78−7.72 (m, 3H, ar), 7.46−7.13 (m, 24H, ar), 4.02 (t, J = 6.5, 2H, OCH_2), 2.25 (dd, J(PH) = 58, J(HH) = 7, 4H, CH_2PPh_2), 1.81−1.10 (m, 11 H, CH_2, CH ali.). ^{13}C NMR ($CDCl_3$): δ 157.0, 138.9, 134.6, 133.0, 132.8, 131.5, 130.7, 129.3, 128.8, 128.4, 127.6, 126.7, 126.3, 123.4, 119.0, 106.5, 67.9, 35.7, 35.3, 35.1, 32.7, 32.6, 32.4, 29.2, 26.0, 25.8 ppm. ^{31}P{^{1}H}NMR ($CDCl_3$): δ −20.4. MS (EI): 638. Anal. Calcd for $C_{43}H_{44}OP_2 \cdot 0.5H_2O$ (647.76): C, 79.73; H, 7.00. Found: C, 79.73; H, 7.04.

{[Pd$_2$(dpppR)$_2$(dmb)]2ClO$_4$}$_n$ (11). 1 (23 mg, 0.0352 mmol), **17** (45 mg, 0.0704 mmol), and $LiClO_4$ (15 mg, 0.1408 mmol) were put in a flask under nitrogen. Distilled water (25 mL) was added to the mixture followed by the addition of dichloromethane (25 mL). The two-layer solution was stirred at room temperature under nitrogen for 2 h. After the stirring, the mixture was extracted with dichloromethane. The organic layer was washed with distilled water, dried over $MgSO_4$, and reduced to 5 mL. Diethyl ether (100 mL) was added to precipitate the product, which was separated by filtration to lead to compound **11** as a yellow solid (20.6 mg, 91%). ^{1}H NMR (CD_2Cl_2): δ 7.81−6.85 (m, 54H, ar), 4.06 (m, 4H, OCH_2), 2.40 (m, 8H, CH_2PPh_2), 1.88−0.80 (m, 40H, CH_2, CH). ^{31}P{^{1}H} NMR (CD_2Cl_2): δ 13.1, −3.0. ^{13}C NMR ($CDCl_3$): δ 157.0, 148.5, 142.2, 138.9, 135.1, 134.8, 134.6, 128.5, 133.0, 132.8, 131.5, 130.7, 129.3, 128.8, 128.4, 127.6, 126.7, 126.3, 123.4, 119.0, 106.5, 67.9, 65.2, 61.9, 44.9, 37.6, 35.7, 35.3, 35.1, 32.7, 32.6, 32.4, 29.2, 28.2, 27.7, 26.0, 25.8, 25.6, 22.4. IR (KBr): 2171 (ν(N≡C)), 1097 (ν(Cl−O)). Anal. Calcd for $C_{98}H_{106}Cl_2N_2O_{10}P_4Pd_2 \cdot CH_2Cl_2 \cdot$0.5acetonitrile (1985.00): C, 60.51; H, 5.56; N, 1.76. Found: C, 60.06; H, 5.61; N, 1.77. The presence of CH_2Cl_2 and acetonitrile was confirmed by ^{1}H NMR and IR.

[Pd$_2$(dppe)$_2$(dmb)$_2$](PF$_6$)$_4$ (12). Excess dmb (192.5 mg, 1.01 mmol) was added to an acetone solution containing [Pd(dppe)(CN-*t*-Bu)$_2$](PF$_6$)$_2$ (242.5 mg, 0.25 mmol). The solution was stirred for 2 h. Diethyl ether was added dropwise until a white precipitate appeared, and 5 mL more of diethyl ether was added. The white powder was washed with diethyl ether and dried under vacuum. Yield: 218 mg (0.18 mmol, 71%). ^{1}H NMR (CD_3CN): 7.70 (m, 40H, Ph), 3.05 (d of t, J = 25.3 Hz, 8H, CH_2P), 1.00−1.80 (complex, 18H, dmb). ^{31}P{^{1}H} NMR (CD_3CN): 76 (s), −137 (septet, PF_6). IR (KBr): 2239 (ν(N≡C), 840 (ν(PF_6)) cm^{-1}. Anal. Calcd for $C_{76}H_{84}N_4P_8F_{24}Pd_2$ (1970.12): C, 46.33; H, 4.30; N, 2.84. Found: C, 46.29; H, 4.44; N, 2.88. UV−vis (CH_3CN): λ_{max} (ϵ) 226 (34700), 248 (24100), 304 nm (7920 M^{-1} cm^{-1}).

Apparatus. All NMR spectra were acquired on a Bruker AC-300 spectrometer (^{1}H 300.15 MHz, ^{13}C 75.48 MHz, ^{31}P 121.50 MHz) using the solvent as chemical shift standard, except in ^{31}P NMR, where the chemical shifts are relative to D_3PO_4 85% in D_2O. All chemical shifts (δ) and coupling constants (J) are given in ppm and Hertz, respectively. The IR spectra were acquired on a Bomem FT-IR MB series spectrometer equipped with a baseline-diffused reflectance. The FT-Raman spectra were acquired on a Bruker RFS 100/S spectrometer. The UV−visible spectra were measured on a HP 8452A diode array spectrophotometer. The time-resolved emission spectra and the emission lifetimes were measured with a nanosecond N_2 laser system from a PTI model GL-3300 pumping a dye laser model GL-302. The pulse width is 2 ns, and the lower limit for the measurements was about 150−200 ps after deconvolution. The excitation wavelength was 400 nm. The continuous wave emission spectra were measured on a SPEX Fluorolog II. The glass transition temperature (T_g) was measured using a Perkin-Elmer 5A DSC7 equipped with a thermal controller 5B TAC 7/DS. Calibration standards were water and indium. The accuracy is ±0.1 °C and ±0.1% for ΔCp. The sample weights ranged from 5 to 10 mg, and

the scan rate was adjusted at 10 deg/min. XRD were acquired on a Rigaku/USA Inc. instrument using copper radiation (Kα). TGA were acquired on a TGA 7 of Perkin-Elmer between 50 and 650 °C at 3 deg/min under nitrogen atmosphere. The MALDI-TOF data were obtained at the Université de Bourgogne (Dijon, France) using a PROFLEX III Bruker spectrometer. This instrument was set in linear mode and used a N_2 laser. The data analysis were performed using a homemade program written in GW BASIC computing all mathematically possible solutions for each fragment mass. Only the chemically meaningful solutions were retained using a window of ±2 g.

Spin−Lattice Relaxation Times (T_1). The T_1s were measured by inversion recovery pulse technique. The measurements were performed on a Bruker AC-F 300 NMR spectrometer operating at 75.47 MHz for ^{13}C. The temperature was 293 K, and the sampling was done over a 20000 Hz sweep width using 8192 data points to describe the FID. The solutions were saturated in all cases in order to improve the signal-to-noise ratio. The uncertainties are of ±0.10 s based upon multiple measurements (at least 3). The second instrument was a Varian 500 MHz instrument located at McGill University. The experimental procedure is the same as above.

Computer Modeling. The calculations were performed using the commercially available PC Model from Serena Software (version 7.0), which uses the MMX empirical model. No constraint on bond distances and angles was applied to ensure that deviations from normal geometry were depicted. The R−N≡C groups were replaced by R−C≡C$^-$ because PC Model does not model the C≡N$^+$− fragments accurately. In fact, strongly bent structures were calculated due to unrealistic electrostatic repulsions (i.e., C≡N$^+$···C≡N$^+$). Instead, −C≡C− was used securing a more linear and realistic frame for the ligand. The $Pd_2(dmb)_2Cl_4$ was modeled and compared to its X-ray structure[8] to provide an idea on the level of adequacy of the method. Selected data (Å, deg) are as follows (the X-ray data are placed in parentheses): d(Pd−C) = 1.93 (1.97), d(C≡N) = 1.14 (1.13), d(Pd−Cl) = 2.23 (2.43), d(Pd···Pd) = 4.51 (4.40), d(Cl···Cl) = 3.54 (3.47), ∠(CPdC) = 178.0 (178.6), ∠(ClPdCl) = 179.2 (178.6), ∠(PdCN) = 177.5 (178.6). This method is qualitative.

Intrinsic Viscosity. The intrinsic viscosity measurements were performed using the universal standard polymethyl methacrylate from Aldrich (M_n = 12000, 15000, 120000, and 320000). The measurements were reproduced 5 times for greater accuracy. The results were checked against the known oligomer $\{[Ag(dmb)_2]BF_4\}_n$ (M_n = 4000).[14]

X-ray Crystallography. Crystals for $[Pd(dppe)(dmb)]_2(PF_6)_4$ were grown by vapor diffusion using *tert*-butyl methyl ether and acetonitrile at 23 C°. Single crystals were coated with Paratone-N oil, mounted using a glass fiber, and frozen in the cold nitrogen stream of the goniometer. A hemisphere of data was collected on a Bruker AXS P4/SMART 1000 diffractometer at the University of New Brunswick, using ω and θ scans with a scan width of 0.3° and 30 s exposure times. The detector distance was 5 cm. The data were reduced (SAINT) and corrected for absorption (SADABS).[15,16] The structure was solved by direct methods and refined by full-matrix least squares on F^2 (SHELXTL).[17] One of the PF_6 ions was disordered. The site occupancies were refined to 0.6 (F(13)−F(15)) and 0.4 (F(16)−F(18)) using an isotropic model and fixed for following refinement cycles. All non-hydrogen atoms were refined anisotropically. Hydrogen atoms were included in calculated positions and refined using a riding model. Crystallographic data are summarized in Table 1, and atomic coordinates, thermal parameters, and bond lengths and angles are included in the Supporting Information.

Table 1. Crystal Data for **12**

formula	$C_{76}H_{84}F_{24}N_4P_8Pd_2$
fw	1970.03
temp, K	173(1)
crystal size	0.15 × 0.25 × 0.40
lattice	monoclinic
space group	*C*2/*c*
a, Å	24.3735(13)
b, Å	21.8576(13)
c, Å	18.0034(9)
α, deg	90
β, deg	119.775(1)
χ, deg	90
V, Å^3	8325.0(8)
Z	4
ρ(calcd), g cm^{-3}	1.572
μ(Mo Kα), mm^{-1}	0.684
F(000)	3984
no. of observns ($I > 2.00\sigma(I)$)	9470
R1[a]	0.0598
wR2[b]	0.1718

[a] $R1 = \sum||F_o| - |F_c||/\sum|F_o|$. [b] $wR2 = (\sum[w(F_o^2 - F_c^2)^2]/\sum[F_o^4])^{1/2}$. Weight = $1/[\sigma^2(F_o^2) + (0.0984P)^2 + (33.1734P)]$, where $P = (\max(F_o^2,0) + 2F_c^2)/3$.

Quantum Yields. The reference for the quantum yield measurements at 77 K was H_2TPP (Φ = 0.11; TPP^{2-} = tetraphenyl porphyrin dianion). This value was obtained with (Pd)TPP (Φ = 0.17; 77 K; MCH (methylcyclohexane)) as reference.[18]

Theoretical Computations. The density functional theory calculations (DFT) were performed using the commercially available Gaussian 98 software[19] and a Pentium 4 (1.6G). The computations for all three, geometry optimization, vibrational frequencies, and frontier molecular orbitals, were performed at the RB3LYP level (Becke's three parameter hybrid functional using the LYP (Lee−Yang−Parr) correlation functional[20,21]). The basic set for the polarization and diffuse function was the 3-21G* set.[22] To save computation time, dmb was replaced by two CNH ligands, and PPh_3 by PMe_3. In the last replacement, PMe_3 was selected instead of PPh_3 in order to keep a mass large enough at the axial position of the Pd−Pd bond due to strong coupling. Tight conversion was used in the computation in order to avoid imaginary vibrational frequencies.

(14) Turcotte, M.; Harvey, P. D. *Inorg. Chem.* **2002**, *41*, 2971.
(15) *SAINT 6.02*; Bruker AXS, Inc.: Madison, WI, 1997−1999.
(16) Sheldrick, G. *SADABS*; Bruker AXS, Inc.: Madison, WI, 1999.
(17) Sheldrick, G. *SHELXTL 5.1*; Bruker AXS, Inc.: Madison, WI, 1997.
(18) Murov, S. L.; Carmichael, I.; Hug, G. L. *Handbook of Photochemistry*, 2nd ed.; Marcel Dekker: New York, 1993.
(19) Frisch, M. J.; Trucks, G. W.; Schlegel, H. B.; Scuseria, G. E.; Robb, M. A.; Cheeseman, J. R.; Zakrzewski, V. G.; Montgomery, J. A., Jr.; Stratmann, R. E.; Burant, J. C.; Dapprich, S.; Millam, J. M.; Daniels, A. D.; Kudin, K. N.; Strain, M. C.; Farkas, O.; Tomasi, J.; Barone, V.; Cossi, M.; Cammi, R.; Mennucci, B.; Pomelli, C.; Adamo, C.; Clifford, S.; Ochterski, J.; Petersson, G. A.; Ayala, P. Y.; Cui, Q.; Morokuma, K.; Malick, D. K.; Rabuck, A. D.; Raghavachari, K.; Foresman, J. B.; Cioslowski, J.; Ortiz, J. V.; Baboul, A. G.; Stefanov, B. B.; Liu, G.; Liashenko, A.; Piskorz, P.; Komaromi, I.; Gomperts, R.; Martin, R. L.; Fox, D. J.; Keith, T.; Al-Laham, M. A.; Peng, C. Y.; Nanayakkara, A.; Gonzalez, C.; Challacombe, M.; Gill, P. M. W.; Johnson, B. G.; Chen, W.; Wong, M. W.; Andres, J. L.; Head-Gordon, M.; Replogle, E. S.; Pople, J. A. *Gaussian 98*, revision A.6; Gaussian, Inc.: Pittsburgh, PA, 1998.
(20) (a) Becke, A. D. Density-functional Thermochemistry. III The Role of Exact Exchange. *J. Chem. Phys.* **1993**, *98*, 5648. (b) Lee, C.; Yang, W.; Parr, R. G. *Phys. Rev.* **1988**, *B 37*, 785.
(21) Miehlich, A. D.; Savin, A.; Stoll, H.; Preuss, H. *Chem. Phys. Lett.* **1989**, *157*, 200.
(22) (a) Dobbs, K. D.; Hehre W. J. *J. Comput. Chem.* **1986**, *7*, 359; (b) *J. Comput. Chem.* **1987**, *8*, 861; (c) *J. Comput. Chem.* **1987**, *8*, 880.

Table 2. Codes for the Investigated Pd-Containing Materials

compound	code	compound	code
$Pd_2(dmb)_2Cl_2$	**1**	$\{[Pd_2(dmb)_2(dpph)](ClO_4)_2\}_n$	**7**
$Pd_2(dmb)_2Cl_4$	**2**	$\{[Pd_2(dmb)_2(dpa)](ClO_4)_2\}_n$	**8**
$Pd_2(CN\text{-}t\text{-}Bu)_4Cl_2$	**3**	$\{[Pd_2(dppe)_2(dmb)](ClO_4)_2\}_n$	**9**
$[Pd_2(dmb)_2(PPh_3)_2](ClO_4)_2$	**4**	$\{[Pd_2(dppp)_2(dmb)](ClO_4)_2\}_n$	**10**
$\{[Pd_2(dmb)_2(dppb)](ClO_4)_2\}_n$	**5**	$\{[Pd_2(dppp\mathbf{R})_2(dmb)](ClO_4)_2\}_n$	**11**
$\{[Pd_2(dmb)_2(dpppen)](ClO_4)_2\}_n$	**6**	$[Pd_2(dppe)_2(dmb)_2](PF_6)_4$	**12**

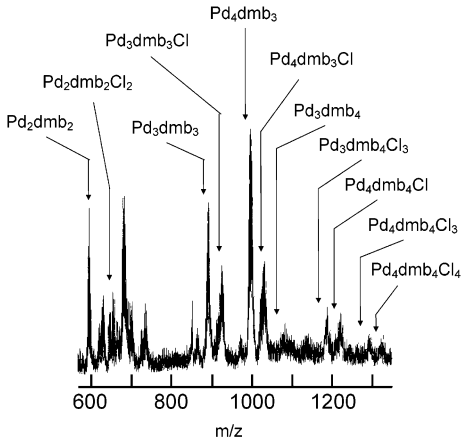

Figure 1. MALDI-TOF spectrum of **1**.

Chart 4

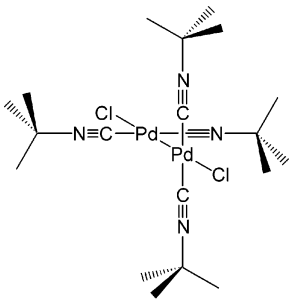

$Pd_2(CN\text{-}t\text{-}Bu)_4Cl_2$ (**3**)

Results and Discussion

During the course of this investigation, the starting material, **1**,[8] was revisited due to new findings suggesting the presence of a structure of a larger dimension in the solid state. Because of this particular property, a broad and systematic characterization of these new materials has been undertaken. Table 2 lists the codes employed for the investigated materials.

I. $Pd_2(dmb)_2Cl_2$ Revisited. Ia. Solid State Properties. The MALDI-TOF spectra exhibit fragment peaks, which indicate that the title compound is not a binuclear complex in the solid state (Figure 1). Instead, the observed peaks suggest that this species contains at least two "$Pd_2(dmb)_2Cl_2$" units. We were unable to grow single crystals suitable for X-ray diffraction experiments. The material is amorphous as determined by XRD measurements (Supporting Information). Further characterization by DSC also indicates the presence of a reproducible glass transition (T_g) at ~6 °C ($\Delta Cp = 1.55$ J/°C; Supporting Information). In addition, the material exhibits a decomposition process that spreads from 120 to 270 °C, based on TGA measurements (Supporting Information). The morphology, the presence of a T_g, and the relatively large temperature range of decomposition are consistent with the presence of a polymeric structure in the solid state.

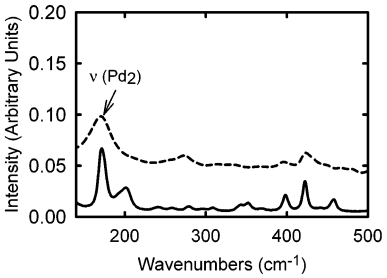

Figure 2. Comparison of the solid state FT-Raman spectra in the low-frequency region of **1** (- - -) and **3** (—).

The comparison of the solid state FT-Raman spectra of **1** with the related and crystallographically characterized **3** (Chart 4),[9] notably for $\nu(Pd_2)$ (Figure 2), indicates that the ClPdPdCl fragment is kept in the polymer. The $\nu(Pd_2)$ values of 170 and 172 cm^{-1} for **3** (this work) and **1**,[23] respectively, support this assignment. In linear XMMX fragments, the $\nu(Pd_2)$, $\nu(PdCl)_{sym}$, and $\nu(PdCl)_{asym}$ modes are strongly coupled.[24] DFT calculations performed on the model compound $Pd_2(CNH)_4Cl_2$ predict that $\nu(Pd_2)$, $\nu(PdCl)_{sym}$, and $\nu(PdCl)_{asym}$ are 167, 294, and 262 cm^{-1}, respectively. The computed value for $\nu(Pd_2)$ (167 cm^{-1}) compares favorably to that experimentally measured for **3** (170) and **1** (172 cm^{-1}). The absence of $\nu(N{\equiv}C)$ associated with uncoordinated CNR groups indicates that this material is either cyclic or a macromolecule of a very large dimension in the solid (i.e., a polymer).

Ib. T_1/NOE Measurements. The solid state data above (MALDI-TOF, DSC, and XRD) suggest that the properties of **1** in solution be carefully revisited, particularly with respect to molecular dimension.[8] Previous FAB mass data for the $Pd_2(dmb)_2X_2$ (X = Cl, Br) in NBA (nitrobenzyl alcohol) indicates the presence of "$Pd_2(dmb)_2X_2$", "$Pd_2(dmb)_2X$", and "$Pd_2(dmb)_2$" as the largest fragments.[8] To confirm this, attempts to measure a molecular weight from the measurements of the intrinsic viscosity, assuming the presence of an oligomer, failed as no time difference is noted between the pure acetonitrile solvent and the saturated solution for **1** and **3** (as a check for the method). This circumstantial evidence can only indicate that the size of the title complex is certainly very small in solution.

Recently this group demonstrated how to use spin−lattice relaxation time and nuclear Overhauser enhancement (NOE) measurements to obtain information about the size of the tumbling molecules in solution for $\{Ag(dmb)_2^+\}_n$.[14] This recent work reports this methodology in detail, and only the key features are presented here. The size of a molecule can be obtained from the Stokes−Einstein−Debye equation assuming a spherical shape if the correlation time, τ_c, is known ($\tau_c = V\eta_{visc}/kT$; η_{visc} = solvent viscosity; k = Boltzmann constant; T = temperature). In order to measure

(23) Harvey, P. D.; Murtaza, Z. *Inorg. Chem.*, **1993**, *32*, 4721.
(24) Herzberg, G. *Molecular Spectra and Molecular Structure;* Van Nostrand: New York, 1945; Vol. 11, p 180.

τ_c, one has to know the spin−lattice relaxation time related to dipole−dipole interactions, T_1^{DD}, which is given by eq 1,

$$1/T_1^{DD} = \sum(h^2\gamma_C^2\gamma_H^2/4\pi^4 r_{CH}^6)\tau_c \quad (1)$$

in the extreme narrowing limit,[25] where h is the Planck constant, γ is the magnetogyric ratio for the interacting nuclei (^{13}C and ^1H in this work),[26] and r is the distance between the probe (here ^{13}C) and the nearest interacting nuclei (here ^1H). The T_1^{DD} data (here at 300 MHz ^1H) can be extracted from experimental T_1 and NOE measurements,[26b] according to eq 2,

$$1/T_1^{DD} = \eta/(\eta_{max}T_1) \quad (2)$$

with η = the fractional NOE constant, η_{max} = the maximum η value in the extreme narrowing limit (here $\eta_{max} = \gamma_H/2\gamma_C = 1.988$), and T_1 is the experimental spin−lattice relaxation time.[27] The strategy is to compare the hydrodynamic volume of a reliably known compound (ideally characterized from crystallography) to that of the unknown ones. One parameter that has to be taken into account is that the standard molecule must be closely related to the sample molecules, not only in terms of structure but also in terms of charge due to the effect of solute−solvent interactions. In this work, the probe nucleus is the quaternary ^{13}C located in the cyclohexane ring because any motion of the tumbling molecule in solution is felt by this nucleus without major interference from unrelated motions, such as CH_3 rotations or cyclohexane conformational changes. In addition, T_1 times associated with quaternary ^{13}C are generally long, hence providing more sensitivity. The quality of the data becomes only a function of the accumulation time. By combining eqs 1 and 2 with the Stokes−Einstein−Debye equation, one obtains

$$\frac{T_1(\text{sam})}{T_1(\text{sta})} = \frac{\eta_{CH}(\text{sam})}{\eta_{CH}(\text{sta})}\frac{V(\text{sta})}{V(\text{sam})}\frac{\sum 1/r_{CH}^6(\text{sta})}{\sum 1/r_{CH}^6(\text{sam})} \quad (3)$$

where "sam" and "sta" stand for sample and standard, respectively. This equation requires the knowledge of the interatomic distances between the ^{13}C probe nucleus and the surrounding ^1H nuclei (Chart 5). The X-ray structure for the standard molecule **2** (standard A) provides this information.[8] This first standard is selected because it exhibits the same "$Pd_2(dmb)_2$" ring as the investigated molecule. By assuming that these separations are the same in **1** and **2**, the term $[\sum 1/r_{CH}^6(\text{sam})]/[\sum 1/r_{CH}^6(\text{sta})]$ becomes unity. **3** is also used as a second standard (standard B) because it exhibits an unsupported Pd_2 single bond along with two axially coordinated Cl atoms. Rotation around this bond is possible, and one may wonder what effect this rotation has on T_1.

Chart 5

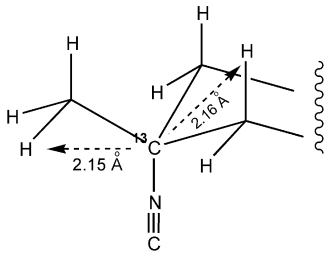

Table 3. T_1 and NOE Data for **1**, **2**, and **3**

compounds	T_1/ ±0.10 s	η_{CH}	$[T_1(\text{sta})\eta_{CH}(\text{sam})]/[T_1(\text{sam})\eta_{CH}(\text{sta})]$	V(sta)[a]/ Å^3	V(sam)[b]/ Å^3
1	8.99	1.32			
2 (standard A)	9.10	1.36	0.982	∼770	∼760
3 (standard B)	9.32	1.54	0.889	∼820	∼730

[a] The volumes are determined with available X-ray structures (V of the unit cell divided by Z). The volume for **2** is calculated from the unit cell volume for **2**·H_2O. Using the density of water, the volume of H_2O is approximated at 30 Å^3. Just for comparison purposes, PC Model computes volumes of 582, 643, and 694 Å^3 for **3**, **1**, and **2**, respectively. [b] $V(\text{sam}) = [(T_1(\text{sam})\eta_{CH}(\text{sta}))/(T_1(\text{sta})\eta_{CH}(\text{sam}))] \times V(\text{sta})$.

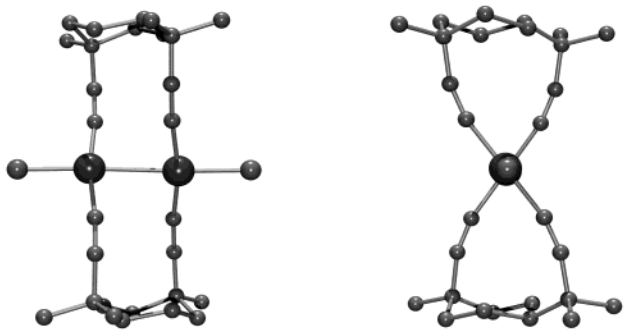

Figure 3. Computer modeling for **1** in solution: (left) showing the Cl−Pd−Pd−Cl axis; (right) showing the dihedral C−Pd−Pd−C angle.

The T_1 and NOE data are summarized in Table 3, and the comparison between **1** and **2** is striking. These values are very similar, which confidently proves the binuclear formulation of the title compound in solution. The estimated volume for **1** (V(sam) = ∼760 Å^3) is also a bit smaller than that of **2**, which is anticipated because of the lower number of Cl atoms. The T_1 and NOE data for **3** are a little different (notably for η_{CH}), but the estimated volume is the about the same (∼730 Å^3). The comparison of these two estimated values with the X-ray data for the two standards (V(sam) < V(standard A) < V(standard B)) is also consistent with the relative order of the calculated molecular volumes using PC Model (see details in the Table 3 foonote). All in all, **1** is a binuclear complex in solution.

Ic. Computer Modeling. Modeling of **1** is used for two qualitative purposes. The first one is to understand what drives the polymer structure in the solid state, and the second one is to suggest what is, and is not, reasonable as possible structures of the title structure in the solid state. The modeled d^9-d^9 binuclear structure where $d(Pd_2)$ is set at 2.60 Å, for instance (Figure 3), exhibits an obvious stress in the "Pd_2-dmb" rings associated with the incompatibility between the

(25) T_1 decreases with the field (H_0) indicating the extreme narrowing limit.
(26) Drago R. S. *Physical Methods for Chemists*, 2nd ed.; Saunders College Publ.: New York, 1992. (b) Wehrli, F. W.; Wirthlin, T. *Interpretation of Carbon-13 NMR Spectra*; Heyden: London, 1980.
(27) The contributions from chemical shift anisotropy, quadrupolar, electron paramagnetic, chemical exchange, and spin-rotation processes are negligible. Indeed, the complex does not exhibit quadrupolar nuclei (except for ^{14}N, which exhibits a very small quadrupolar constant: 2×10^{-26} cm^2),[25] nor are they paramagnetic. The fwhm (full-width-at-half-maximum) was not strongly temperature dependent between 20 and 40 °C.

Chart 6

face-to-face tetrahedral

Chart 7

Top view

Side view

dmb bite distance (4.4 Å seen for **2**)[8] and the Pd_2 single bond length. The computed PdCN (~165°) and CNC (~164°) angles deviate significantly from linearity. These computed angles differ from that of the non-Pd_2-bonded d^8-d^8 complex **2** where no stress is observed, but the smaller MCN angle is not uncommon for dmb. In the $\{Ag(dmb)_2^+\}_n$ polymers, AgCN angles on the order of 161.3(10)° and 162.3(9)° have been reported.[7] In these latter cases, dmb−dmb steric hindrance causes these important deviations. On the other hand, the experimental CNC angle in these $\{Ag(dmb)_2^+\}_n$ polymers has never decreased below 170°.[7] Nonetheless, the computations for **1** (for an isolated molecule) suggest clearly that ring stress is present. In the solid state, this ring stress may drive the ligand reorganization toward polymerization where lesser stress is predicted.

Possible solid state structures such as a dimer, $(\mathbf{1})_2$, are also considered. Two structures are considered: the "face-to-face" and "tetrahedral" geometries (Chart 6). The "face-to-face" structure is similar to that of **2**, except the $PdCl_2$ unit is replaced by a linear Pd_2Cl_2 fragment placing the Pd−Pd axes parallel to each other, and involves two pairs of μ-dmb ligands placed alongside each other above and beneath the Pd−Pd bonds. This geometry induces important dmb−dmb steric interactions, where unrealistic distortions are noted. The considered "tetrahedral" geometry places the ClPdPdCl axes perpendicular to each other, one above the other, and has the 4-dmb ligands occupying the 4 other vertexes of the tetrahedron. Again, unrealistic distortions are observed in these computed models as the size of the dmb bite angle is incompatible with the Pd_2 bond length.[28] Computer modeling indicates clearly that the "dimer-of-binuclear complex" formulation in the solid state (i.e., $[Pd_2(dmb)_2Cl_2]_2$) is highly implausible.

(28) Other geometries where the ClPdPdCl fragment is not linear were also considered, but similar results about large distortion were observed.

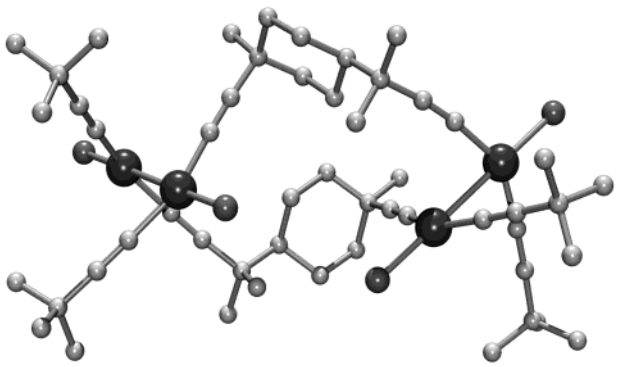

Figure 4. Computer modeling for "$Pd_4(dmb)_2(CN\text{-}t\text{-}Bu)_4Cl_4$" representing a segment of a plausible 1-D polymer.

One possible geometry for a $\{\mathbf{1}\}_n$ polymer is the 1-D structure. This possibility is considered because of the existence of the doubly bridged $\{M(dmb)_2^+\}_n$ materials (M = Cu, Ag),[4] and the recently discovered "polymer of dimer" $\{M_2(dppm)_2(dmb)_2^+\}_n$.[5] A computer modeling for "$Pd_4(dmb)_2(CN\text{-}t\text{-}Bu)_4Cl_4$" representing a segment of a plausible 1-D $\{\mathbf{1}\}_n$ polymer structure (Chart 7) is shown in Figure 4. In this structure, no ring stress is apparent, and dmb adopts the *Z*-conformation. The CPdC angles are closer to the ideal angles of 180° and agree with the structure for **3**.[9] Despite this interesting result, 2- and 3-D structures cannot be ruled out.[29] Because of the amorphous nature of the materials, the structure cannot be deduced, but modeling suggests a clear explanation for the preferred polymeric structure in the solid.

II. The $[Pd_2(dmb)_2(PPh_3)_2](ClO_4)_2$ Complex (4). IIa. Synthesis and Characterization. This complex is synthesized according to eq 4:

(29) Examples of 2- and 3-D polymers of diisocyanide are also known. See for examples: (a) Dartiguenave, M.; Dartiguenave, Y.; Mari, A.; Guitard, A.; Olivier, M. J.; Beauchamp, A. L. *Can. J. Chem.* **1988**, *66*, 2386. (b) Guitard, A.; Mari, A.; Beauchamp, A. L.; Dartiguenave, Y.; Dartiguenave, M. *Inorg. Chem.* **1983**, *22*, 1603.

$$Pd_2(dmb)_2Cl_2\ (\mathbf{1}) + 2PPh_3 + 2LiClO_4 \rightarrow [Pd_2(dmb)_2(PPh_3)_2](ClO_4)_2\ (\mathbf{4}) + 2LiCl \quad (4)$$

The air-stable red product exhibits a single ^{31}P NMR resonance at 24.2 ppm and a strong ν(NC) absorption at 2170 cm^{-1} consistent with CNR groups coordinated onto a Pd(I) center.[8,9] Contrarily to the related axially functionalized d^9-d^9 $Pd_2(CNR)_4(PPh_3)_2^{2+}$ cations (R = Me, *t*-Bu),[30] **4** does not exhibit any fluxional processes on the basis of ^1H and ^{31}P NMR findings. This absence of fluxion is presumably due to its bridged structure, which renders the CNR/PR_3 exchange impossible. This binuclear complex also bears similarities with the $Pd_3(CNMe)_6(PPh_3)_2^{2+}$ trimer[31] and $M_4(dmb)_4(PPh_3)_2^{2+}$ (M = Pd, Pt)[6] for which the phosphines are also placed at the axial position of the M_n axes. The complex is soluble in most common organic solvents such as acetonitrile, acetone, dichloromethane, and tetrahydrofuran. The binuclear structure in solution is easily confirmed by T_1 (8.35 s) and NOE (1.43) measurements, in comparison with data for the above standard compounds **2** and **3** (neglecting the presence of the charge on the binuclear complex). The smaller T_1 is perfectly consistent with the greater volume of **4**.

Similarly to **1**, the MALDI-TOF data (Supporting Information) exhibit fragment peaks consistent with the presence of a larger dimension species in the solid state, and the XRD traces reveal the presence of an amorphous solid. The similarity in solid state and solution properties between this species (**4**) and its precursor **1** also suggests the presence of stress in the "$Pd_2(dmb)_2$" rings inducing the dissociation and reorganization of dmb between the two phases. In contrast, no T_g is observed (between 25 and 190 °C; DSC).

IIb. Geometry Optimization and Modeling for 4. In the absence of an X-ray structure, and because of the need to interpret the UV−visible and FT-Raman spectra below, the geometry of a model compound, $Pd_2(CNH)_4(PMe_3)_2^{2+}$ (in the "gas phase") was computed by means of DFT (RB3LYP; basis set 3-21G*). At convergence, the model exhibits the expected Pd_2-bonded binuclear complex with a 90° angle between the "$Pd(CNH)_2$" planes (D_{2d} local point group). The PMe_3 ligands place themselves in such a way that one dihedral CPPd(CN) angle of 0° is obtained for each half of the molecule (D_2 point group). The calculated distances are as follows: $d(Pd_2)$ = 2.618, d(PdP) = 2.463, d(PdC) = 2.020, d(PC) = 1.834, and d(CN) = 1.167 Å. The calculated $d(Pd_2)$ is exactly where it is expected to be when compared with experimental data for other related binuclear complexes such as $Pd_2(dppm)_2Cl_2$ (2.661(1)),[32] **3** (2.532(2)),[9] and $Pd_2(CNMe)_6^{2+}$ (2.531(1) Å), just to state a few examples.[33] While the other computed distances are normal, d(PdP) is longer than expected. For instance, the d(PdP) data found for other linear axially coordinated polynuclear complexes such as in $Pd_4(dmb)_4(PPh_3)_2^{2+}$ are 2.373 and 2.357 Å;[6] in $Pd_2(PMe_3)_6^{2+}$, it is 2.371;[34] and the $d(PtP)_{axial}$ value reported for the related d^9-d^9 cation $[Pt_2(dppm)_2Cl(PPh_3)]^+$ (if one assumes that the structural data for Pd can be compared to Pt on the basis of the similarity in atomic radii) is 2.333(8) Å.[35]

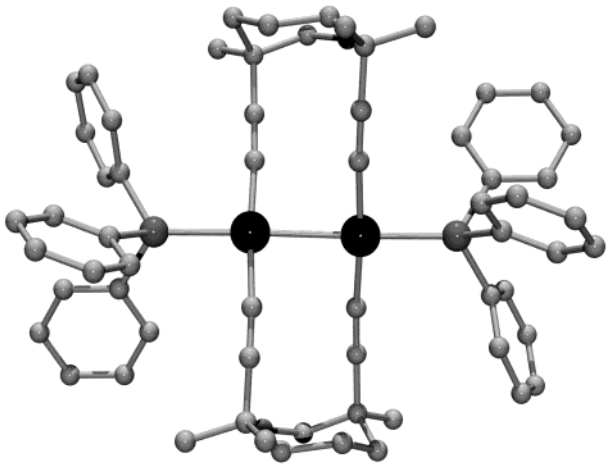

Figure 5. Computer modeling for **4** showing the Pd_2 axis.

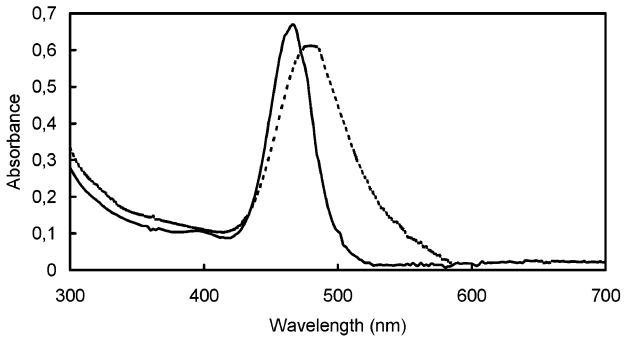

Figure 6. UV−vis spectra of **4** in PrCN at 298 (- - -) and 77 K (—).

Computer modeling for **4** indicates that the molecule belongs to the C_2 point group (Figure 5), ignoring the head-to-tail geometry of dmb with a C_2 axis passing through the Pd_2 bond. In addition, the model with $d(Pd_2)$ and d(PdP) set at 2.62 and 2.42 Å for instance (as close as possible from DFT results) exhibits similarities with **1**, where the PdCN and CNC angles average ∼170° and ∼168°, respectively. The CPK model shows some weak contacts between the Ph rings and dmb suggesting the presence of minor steric hindrance (Supporting Information).

IIc. UV−Visible Spectra and Frontier Molecular Orbitals. The UV−visible spectra are characterized by a strong and narrow absorption at about 482 nm at 298 K (ϵ = 24800 M^{-1} cm^{-1}) which undergoes an evident decrease in bandwidth with the lowering of the temperature (Figure 6: λ_{max} at 298 K = 482 nm, fwhm = 2900 cm^{-1}; λ_{max} at 77 K = 475 nm, fwhm = 2200 cm^{-1}). An M_2-centered electronic transition of the type $d\sigma \rightarrow d\sigma^*$ is a likely candidate for assignment. Electronic bands associated with $d\sigma \rightarrow d\sigma^*$

(30) (a) Boehm, J. R.; Balch, A. L. *J. Organomet. Chem*. **1976**, *112*, C20. (b) Boehm, J. R.; Balch, A. L. *Inorg. Chem*. **1977**, *16*, 778.
(31) Balch, A. L.; Boehm, J. R.; Hope, H.; Olmstead, M. M. *J. Am. Chem. Soc.* **1976**, *98*, 7431.
(32) Besenyei, G.; Parkanyi, L.; Gacs-Baitz, E.; James, B. R. *Inorg. Chim. Acta* **2002**, *327*, 179.
(33) (a) Goldgerg, S. Z.; Eisenberg, R. *Inorg. Chem*. **1976**, *15*, 535. (b) Doonan, D. J.; Balch, A. L.; Goldberg, S. Z.; Miller, J. S. *J. Am. Chem. Soc*. **1975**, *97*, 1961.
(34) Lin, W.; Wilson, S. C.; Girolani, G. S. *Inorg. Chem*. **1994**, *33*, 2265.
(35) Blau, R. J.; Espenson, J. H.; Kim, S.; Jacobson, R. A. *Inorg. Chem*. **1986**, *25*, 757.

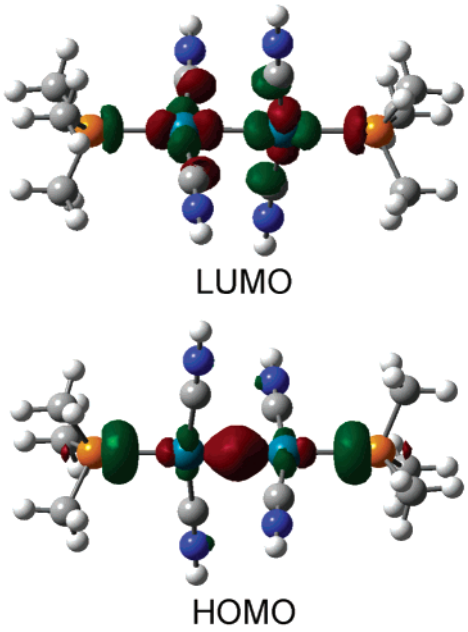

Figure 7. MO drawings of the HOMO and LUMO for the model $Pd_2(CNH)_4(PMe_3)_2^{2+}$.

electronic transitions for M_2-bonded species generally exhibit low energies and high intensities ($\epsilon > 10000$ M^{-1} cm^{-1}) and are often narrow ($2000 <$ fwhm < 4000 cm^{-1} at room temperature).[36,37] The most striking piece of evidence for such a band in the UV−vis spectra is the high sensitivity of the λ_{max} and fwhm with the temperature. Upon cooling the samples, either in the solid state or in solution, the $d\sigma \rightarrow d\sigma^*$ bands experience a significant blue shift and decrease in fwhm. This well-known phenomenon is due to lower energy "hot bands" of vibronic origin, which disappear upon cooling.[36,37] The presence or absence of such hot bands depends on the vibrational frequency of the Franck−Condon active modes in the electronic transitions. For $d\sigma \rightarrow d\sigma^*$ transitions, this mode is $\nu(M_2)$, which is generally of low frequency, leading to significant hot band contributions in the $d\sigma \rightarrow d\sigma^*$ spectral envelope. For MLCT or d−d transitions, higher frequency Franck−Condon active modes are generally present, such as intraligand and M−L stretches. Because of their greater energy gap, the higher vibrational levels are not heavily populated. As a consequence, there is no or little intensity arising from hot bands and, upon cooling the samples, the band shape does not change greatly and the hot bands' intensity is weak or nil.

In order to support this assignment, DFT calculations were performed on the HOMO and LUMO of the model compound $Pd_2(CNH)_4(PMe_3)_2^{2+}$ (Figure 7). The LUMO (5.67 eV) and HOMO (2.22 eV) exhibit the anticipated $d_{x^2-y^2}\cdots d_{x^2-y^2}$ interactions arising from T-shaped ML_3 fragments,[38] leading to $d\sigma^*$- and $d\sigma(Pd_2)$ orbitals, respectively. In addition, these frontier orbitals exhibit P lone pair contributions leading in both cases to antibonding Pd−P interactions. Using both D_{2d} local (ignoring the PMe_3 orientations) and D_2 point groups (considering that the "$Pd(CNR)_2$" planes may not be 90°), the symmetry of the HOMO and LUMO is a_1 and b_2, and a_1 and b_1, respectively. Hence, the ground and lowest energy excited singlet and triplet excited states are $^1A_1$ and $^{1,3}B_2$, and $^1A_1$ and $^{1,3}B_1$, respectively. The lowest spin-allowed electronic transition is allowed by symmetry for both point groups, and the transition moment is polarized along the *z*-molecular axis (Pd−Pd bond).

IId. Raman Spectra. The Raman spectra are investigated to localize $\nu(Pd_2)$ and $\nu(PdP)_{sym}$. The solid state Raman spectra in the low-frequency region for **4** is dominated by two strong scattering bands at 119 and 180 cm^{-1}. At first glance these frequencies resemble that seen in Figure 1, but DFT calculations on the model complex $Pd_2(CNH)_4(PMe_3)_2^{2+}$ predict that $\nu(Pd_2)$, $\nu(PdP)_{sym}$, and $\nu(PdP)_{asym}$ are 115, 205, and 157 cm^{-1}, respectively. While the computed $\nu(Pd_2)$ value compares favorably to that of 119 cm^{-1}, the calculated $\nu(PdP)_{sym}$ datum appears off. This is easily explained by the use of the lighter PMe_3 groups instead of PPh_3 ligand in order to save computation time. The assignment for $\nu(Pd_2)$ is further supported by the comparison with $\nu(Pd_2)$ for the related complex $Pd_3(CNMe)_6(PPh_3)_2^{2+}$ [31] (90 cm^{-1}).[39] In addition, the Raman spectra of $PdPt(dppm)_2Cl_2$ and $[PdPt(dppm)_2(\eta^1\text{-dppm})Cl]PF_6$ have been investigated by this group, placing $\nu(PdPt)$ at 154 and 138 cm^{-1}, respectively.[40] Assuming that the decrease in $\nu(PdPt)$ for the replacement of one Cl ligand by a phosphine group (16 cm^{-1}) can also apply for a second substitution, then the predicted $\nu(PdPt)$ value would be 122 cm^{-1} (138−16 = 122). The assignment of the 119 cm^{-1} peak to $\nu(Pd_2)$ for **4** appears reasonable.

III. The $\{[Pd_2(dmb)_2(diphos)](ClO_4)_2\}_n$ Polymers. The syntheses of these materials proceed as described above for **4** (eq 4 and Scheme 1) where the 2 PPh_3 ligands are replaced with diphos (dppb, dpppen, dpph, and dpa). Their identity has been confirmed by the comparison with the NMR (^1H, ^{31}P), and vibrational spectral data ($\nu(N\equiv C)$, $\nu(PdP)$, and $\nu(Pd_2)$) for **4** (see details in the Experimental Section). The signature of the Pd_2 bond (position of the $d\sigma \rightarrow d\sigma^*$ band, and fwhm vs temperature) is also observed as for **4** (Table 4), meaning that the $Pd_2(CNR)_4(P)_2^{2+}$ chromophore is still intact in these materials.

The TGA traces exhibit the presence of two thermal events. The first weight loss ($170 < T_{dec} < 140$ °C) corresponds to the loss of dmb, while the second one ($260 < T_{dec} < 400$ °C) is due to the diphosphine loss (the details of these analyses are available in the Supporting Information). These assignments have been verified using compounds such as **1** and $Pd_2(dppm)_2Cl_2$. The relative weight losses also correspond well, within the uncertainties, to the relative ligand stoichiometry of the materials. The key information is the spread in decomposition temperature. This spread is

(36) Miskowski, V. M.; Smith, T. P.; Loehr, T. M.; Gray, H. B. *J. Am. Chem. Soc.* **1985**, *107*, 7925.
(37) Bersuker, I. B. *Electronic Structure and Properties of Transition Metal Compounds; Introduction to the Theory*; Wiley: New York, 1996; p 337.
(38) Albright, T. A.; Burdett, J. K.; Whangbo, M.-H. *Orbital Interactions in Chemistry*; Wiley: New York, 1985; p 339.
(39) Clark, R. J. H.; Sourisseau, C. *Nouv. J. Chim.* **1980**, *4*, 287.
(40) Evrard, D.; Lucas, D.; Hanquet, B.; Decken, A.; Knorr, M.; Mugnier, Y.; Harvey, P. D. Submitted for publication.

Scheme 1

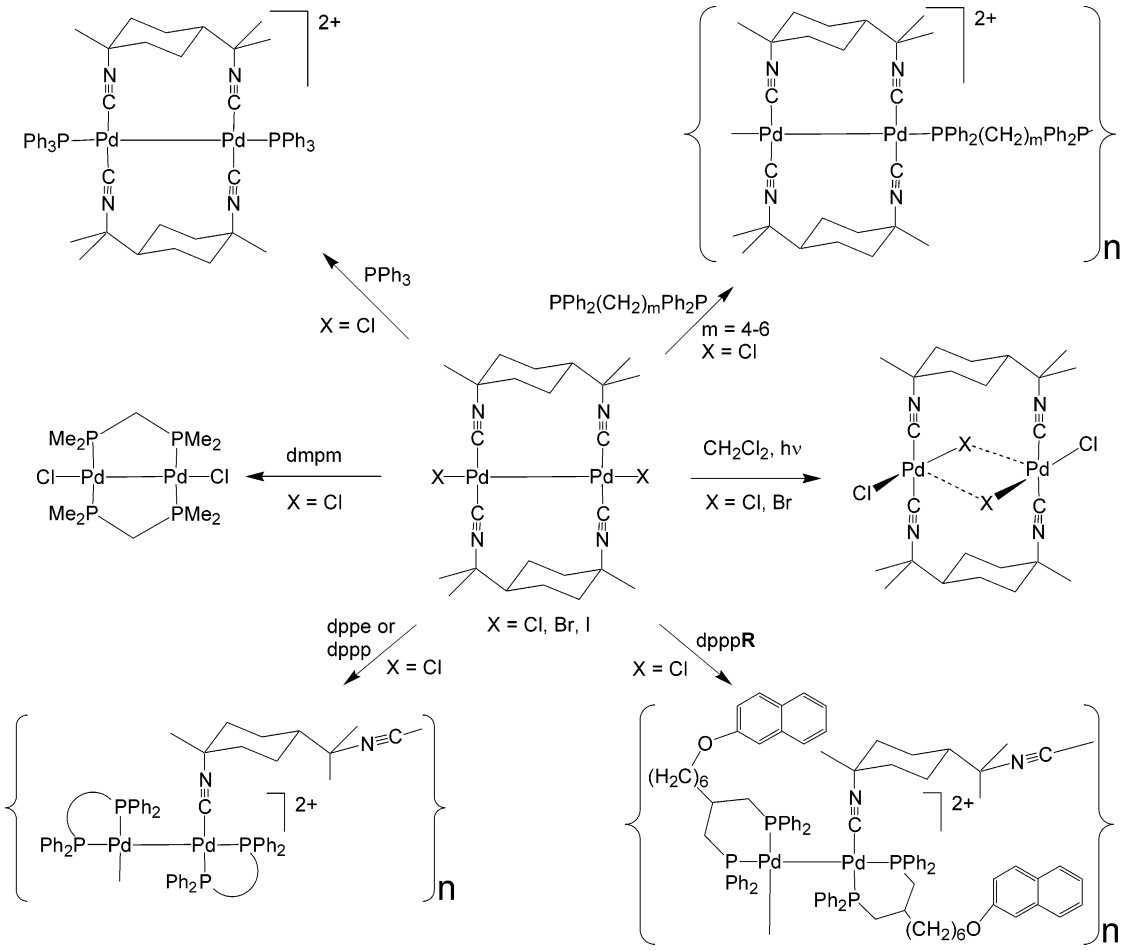

Table 4. Comparison of the UV−Vis Data for **4**, **5**, **6**, **7**, **8**, and **11**

	293 K					77 K	
	ACN			PrCN		PrCN	
compound	λ_{max}/ nm	ϵ/ M^{-1} cm^{-1}	fwhm/ cm^{-1}	λ_{max}/ nm	fwhm/ cm^{-1}	λ_{max}/ nm	fwhm/ cm^{-1}
4	482	24800	2900	486	2900	475	2200
5	486	25400	2700	490	2700	480	2300
6	490	26700	2600	492	2600	484	2400
7	494	26300	2900	498	2900	485	2300
8	492	27100	2700	494	2700	488	2400
11	394	25200	2800	400	2800	390	2500

Table 5. Comparison between T_1/NOE and Intrinsic Viscosity Data

			no. of units	
polymer	$[\eta]$ cm^3 g^{-1}	M_n	intr visc	T_1/NOE
5	4.54	17800	∼14	∼4
6	4.69	18400	∼14	∼4
7	4.10	16100	∼12	∼4
8	4.98	19500	∼16	∼5
9	3.00	11800[a]	∼8[a]	∼2
10	3.09	12100[a]	∼8[a]	∼2
11	3.46	13600	∼7	∼2

[a] From ref 12.

about 50 to 60 °C for the loss of dmb, but ranges between about 100 and 150 °C for the diphosphines (Supporting Information). The large spread is consistent with the presence of a polymer in the solid state.

The dppb, dpppen, and dpph solids are amorphous, as very broad bands (i.e., halo features) are observed in the XRD patterns. On the other hand, the dpa analogue exhibits some sharp peaks superposed on the broad bands, indicative of some degree of crystallinity (i.e., semicrystalline material; Supporting Information). These materials make invariably stand-alone films taking the form of flakes upon the removal of the solvent. For all cases, DSC scans reveal no T_g between 25 °C and the decomposition temperature.

The M_n data (intrinsic viscosity measurements) indicate that these species are oligomers in solution containing about 12−16 units (Table 5). These values are larger than that found for the recently reported $\{[Pd_2(diphos')_2(dmb)^{2+}\}_n$ polymers (about 8; diphos′ = dppe (**9**), dppp (**10**); Scheme 1). The difference is that **5**, **6**, **7**, and **8** exhibit Pd−P axial coordination, while **9** and **10** have Pd−CN bonds. This comparison may indicate the slightly better lability of the dmb ligand vs diphosphines.

IV. The $\{[Pd_2(dpppR)_2(dmb)](ClO_4)_2\}_n$ Polymer. IVa. Synthesis of dpppR. This material has been synthesized to answer two questions. What is the effect of adding lateral chains to the coordination polymer skeleton? And, will the presence of flexible lateral chains affect the analyses of the T_1/NOE data? The choice of the propane chain is due to the commercial availability of the starting materials, in order to limit the number of steps. The synthesis of dppp**R** is shown

Scheme 2

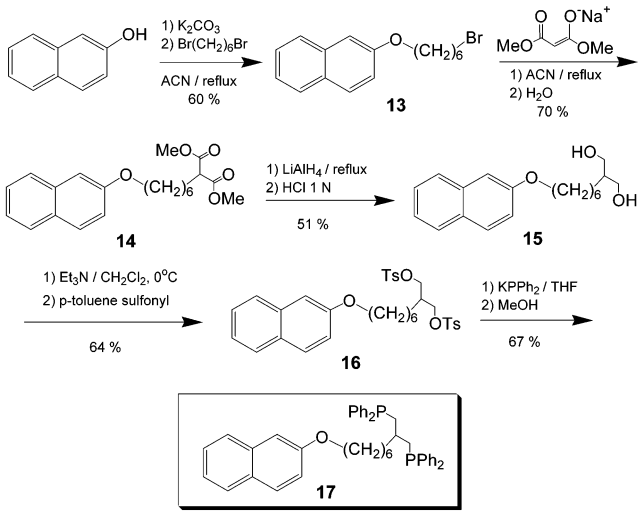

in Scheme 2 and proceeds in 5 steps from 2-naphthol and 1,6-dibromohexane as starting materials. The overall yield from 1,6-dibromohexane to dppp**R** is modest (17%). The dppp**R** ligand is characterized by a single resonance at −20.4 ppm in the ^{31}P NMR spectrum.

IVb. Synthesis of $\{[Pd_2(dpppR)_2(dmb)](ClO_4)_2\}_n$ (11). The material is prepared by reacting the dppp**R** ligand with $Pd_2(dmb)_2Cl_2$ in the presence of $LiClO_4$ (similar to that illustrated in Scheme 1 for diphos′ = dppe and dppp). The new orange material exhibits a strong IR absorption at 2165 cm^{-1} attesting to the presence of coordinated ν(N≡C), two single resonances at +18.3 and +0.9 ppm in the ^{31}P NMR spectra, consistent with a chelated diphosphine at the axial and equatorial positions, and a d$\sigma \rightarrow$ dσ^* band at 394 nm (ϵ = 25200 M^{-1} cm^{-1}) in the UV−vis spectrum, similar to that reported for the **9** and **10**.[12]

The solid is also amorphous (XRD patterns), and the TGA traces exhibit two similar thermal events described for **5**, **6**, **7**, and **8**, associated with the loss of dmb and dppp**R** at low and high temperatures, respectively. The spread of temperature ranges at which the weight losses take place is particularly large (130−290 and 320−460 °C), consistent with the presence of a polymer in the solid state.

The intrinsic viscosity measurements reveal the presence of an oligomer in solution containing about 7 units (M_n = 13600; Table 5). This result indicates that the presence of long lateral chains does not greatly affect the nature of the species in solution when compared to the $\{Pd_2(diphos')_2(dmb)^{2+}\}_n$ species (diphos′ = dppe, dppp), consistent with the fact that the donor properties of dppp and dppp**R** are almost identical. This observation further supports the hypothesis that the relative lability of the dmb and diphosphines controls the size of the oligomers in solution.

The DSC traces exhibit a T_g at 73 °C (scan rate 10 °C/min) with a ΔCp of 2.24 J/g °C. This result contrasts with that of the $\{Pd_2(diphos')_2(dmb)^{2+}\}_n$ materials, which do not exhibit any T_g between 25 and 160 °C, and illustrates the effect of lateral chains on the thermal properties of the solid.

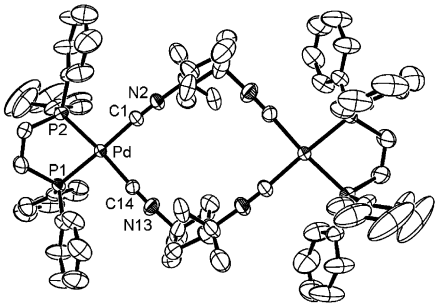

Figure 8. Thermal ellipsoid plot for compound **12**. The ellipsoids are shown at 30% probability. The counterions and the H atoms are not shown for clarity. Selected bond distances (Å) and angles (deg): d(Pd−C(1)) = 2.017(4), d(Pd−C(14)) = 2.022(4), d(Pd−P(1)) = 2.2668(10), d(Pd−P(2)) = 2.2707(11), d(C(1)−N(2)) = 1.117(6), d(N(13)−C(14)) = 1.133(6), ∠C(1)−Pd−C(14) = 90.58(19), ∠C(1)−Pd−P(1) = 177.34(13), ∠C(14)−Pd−P(1) = 91.99(12), ∠C(1)−Pd−P(2) = 94.74(14), ∠C(14)−Pd−P(2) = 174.10(13), ∠P(1)−Pd−P(2) = 82.72(4), ∠N(2)−C(1)−Pd = 176.3-(5), ∠N(13)−C(14)−Pd = 175.7(4).

The XRD pattern reveals a halo feature centered at ∼15°, consistent with an amorphous material, with some weaker fine structures, suggesting the presence of crystalline parts in the solid.

V. T_1/NOE Measurements. Va. Synthesis and Characterization of $[Pd_2(dppe)_2(dmb)_2]^{4+}$. While **4** is an obvious choice of standard in T_1/NOE measurements for **5**, **6**, **7**, and **8**, the choice for a standard for **9**, **10**, and **11** is more limited. Binuclear complexes of the type $Pd_2(diphos')_2(CN\text{-}t\text{-}Bu)_2^{2+}$ are known, but their stability in solution is rather limited.[12] Instead, the new and stable dimer, **12**, has been prepared and fully characterized, despite the presence of a larger charge on the metal. Its synthesis consists of reacting $[Pd(dppe)(CN\text{-}t\text{-}Bu)_2](PF_6)_2$ with dmb in excess, to produce a white microcystalline solid in good yield. The chemical shift of the ^{31}P nuclei is 76 ppm, and the IR spectra show a strong absorption at 2239 cm^{-1} for the coordinated CN group. Both data are consistent with a Pd(II) center.

The identity of this compound is confirmed by X-ray crystallography. The structure consists of two Pd(dppe) fragments, where the dppe chelates the metal, bridged twice by dmb ligands (Figure 8); it can also be viewed as a dimer of "Pd(dppe)(dmb)$^{2+}$". The "$Pd_2(dmb)_2$" macrocycle forms a stair-shaped structure, which is reminiscent of that of $Pd_2(tmb)_2Cl_4$ (tmb = 2,5-diisocyano-2′,5′-dimethylhexane).[8] The square planar geometry of the Pd(II) center is obvious, where the CPdC, PPdC, PPdP, and CPdP angles are 90.58-(19)°, 91.99(12)°, 94,74(14)°, and 82.72(4)°, respectively. The Pd−C (average = 2.020) and Pd−P (2.2688 Å) bond distances are normal (see details in the Supporting Information).

VI. T_1/NOE Measurements of the Polymers. The overall data are presented in Table 6. The T_1 data for the standards **4** (8.35 s; standard C) and **12** (8.16 s; standard D) compare favorably with each other, consistent with the binuclear nature of the complexes. The smaller T_1 for standard B is consistent with the greater dimension of the molecule; PC Model computes volumes of 1226 and 1522 Å^3 for standards C and D, respectively.

Table 6. T_1 and NOE Data for **4**, **5**, **6**, **7**, **8**, **9**, **10**, **11**, and **12**

compound	T_1/ ±0.10 s	η_{CH}	$[T_1(sam)\eta_{CH}(sta)]/[T_1(sta)\eta_{CH}(sam)]$	V^a/ Å^3	V(sta)/ V(sam)	no. of units[b]
4 (std C)	8.35	1.43		1226		
5	2.54	1.66	0.26	1125	1.09	4.2
6	2.46	1.61	0.26	1152	1.06	4.1
7	2.63	1.70	0.26	1174	1.04	4.0
8	2.54	1.89	0.23	1059	1.16	5.0
12 (std D)	8.16	1.37		1522		
9	5.92	1.47	0.68	1260	1.21	1.8
10	4.65	1.46	0.53	1340	1.14	2.1
11	3.81	1.78	0.36	1928	0.79	2.2

[a] Calculated using PC Model since X-ray data are not available for all compounds (except **12**). These values are used solely to estimate the number of units according to the T_1/NOE method. Hence, V(sta)/V(sam) is also calculated from PC Model results. **4** (standard C) is the standard for **5**, **6**, **7**, and **8**, and **12** (standard D) is the standard for **9**, **10**, and **11**. [b] The number of units is calculated from $[(T_1(sta)\eta_{CH}(sam))/(T_1(sam)\eta_{CH}(sta))][V(sta)/V(sam)]$.

The T_1 data can be separated into two groups: (1) **5**, **6**, **7**, and **8** ($2.46 < T_1 < 2.63$ s) and (2) **9**, **10**, and **11** ($3.81 < T_1 < 5.92$ s), consistent with the larger dimension of the former series. The number of units is estimated from the comparison of V(sam) and V(sta), extracted from a modification of eq 3:

$$\text{no. of units} = [(T_1(sta)\eta_{CH}(sam))/(T_1(sam)\eta_{CH}(sta))][V(sta)/V(sam)] \quad (5)$$

The striking feature is the discrepancy between the numbers of units estimated from the measurements of T_1/NOE (shorter) and intrinsic viscosity (longer), where a ratio of 3 to 4 is observed (Table 5). By examining the literature, examples for which the number of units was correctly estimated include systems such as the $\{Ag(dmb)_2^+\}_n$ polymers[14] and the dimer of rhodium(I) complexes of diphosphinated calix[4]arenes.[41] These systems exhibit obvious molecular rigidity induced by multiple cycles within the molecular backbone. As a consequence, τ_c is related to the tumbling of the whole molecule only. For the oligomers $\{Pd_2(dmb)_2(diphos)^{2+}\}_n$, the "local" motions of the rigid metallic "$Pd_2(dmb)_2$ fragments" induce extra processes for dipole−dipole relaxation, so the observed T_1 is averaged out over all the possible motions in solutions (Chart 8).

The flexibility of the $(CH_2)_m$ chains ($m = 4-6$) is obviously responsible for this effect, but the number of units evaluated by T_1/NOE is surprisingly constant with m. This result suggests that the effect of the flexibility is not felt for larger values of m, or very flexible systems. Indeed, in a previous study on the $\{[Pt_4(dmb)_4(diphos)]^{2+}\}_n$ polymers (diphos = dppb, dpppen, dpph; $M_n > 84000$; number of units > 40), the T_1 datum for $Pt_4(dmb)_4(PPh_3)_2^{2+}$ (≈2000 g/mol; 3.76 s) was just barely 2-fold larger than that of the polymers (1.69−2.26 s).[6b] The comparison with **9** and **10** is also intriguing since dmb exhibits less flexibility, and yet, the amplitude of discrepancy is the same, indicating that rotations around the C−C single bonds and −C═N− groups are facile (Chart 9). In order to support this latter hypothesis, **8** is investigated, and the data lead to similar observation, i.e., the ratio between the number of units determined from the measurements of T_1/NOE and the intrinsic viscosity remains the same (3 to 4). To support this model further, **11** is examined as well. As expected, the presence of long flexible lateral chains does not change this ratio.

All in all, the presence of flexibility in the backbone of the oligomers or polymers induces supplementary degrees of freedom to molecular motion, which renders the T_1/NOE method for determining the dimension of the material inadequate.

VII. Photophysical Properties. All investigated complexes and oligomers listed in Table 2 are luminescent neither in solution nor in the solid state at room temperature. This property may be associated with an energy wasting photoinduced homolytic Pd_2-bond scission or ligand dissociation in the excited state. However, the compounds become luminescent at 77 K (in *n*-PrCN). **5**, **6**, **7**, and **8** exhibit emission maxima (λ_{max}) between 627 and 638 nm (Table 7, and Figure 9 as one example). The excitation spectra superimpose the absorptions relatively well, indicating that the absorbing and emitting species are the same. The emission λ_{max} data are more red-shifted in comparison with those observed for **9**, **10**, and **11** ($500 < \lambda_{max} < 509$ nm), which is consistent with the more blue-shifted $d\sigma \rightarrow d\sigma^*$ absorptions of the latter materials (**9** ($\lambda(d\sigma-d\sigma^*) = 414$),[12] **10** (400),[12] **11** (390 nm)). The Stokes shifts (difference

Chart 9

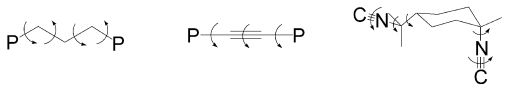

Chart 8

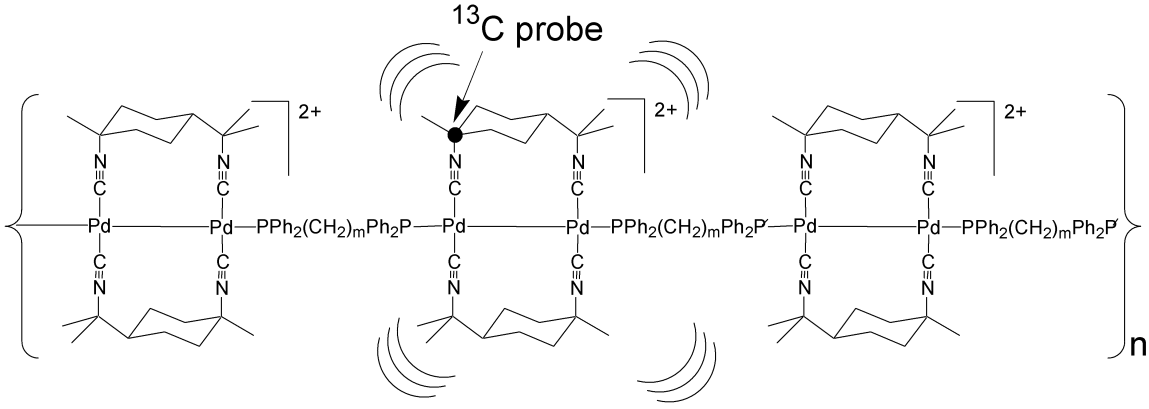

Table 7. Spectroscopic and Photophysical Data for the Oligomers in PrCN at 77 K

compound	λ_{max}/ nm	Δ/ cm^{-1} [a]	τ_e/ ns	Φ[c]
4	627	4900	2.75[b]	0.14
5	632	5100	1.87[b]	0.026
6	634	5200	2.70[b]	0.071
7	636	4900	2.24[b]	0.046
8	638	4800	2.30[b]	0.15
9	509	4500	1.94	0.13
10	508	5300	1.50	0.12
11	500	5600	1.98	0.17

[a] Stokes shift ($\pm$100 cm^{-1}). [b] The decay traces are biexponential, and the uncertainties are $\pm$0.08 ns. The second component is weak (<10%), and the lifetime is on the order of 3 to 5 ns. Because of the weak intensity of this component and the similarity in lifetimes, this second feature is very difficult to reproducibly quantify. [c] $\pm$10%.

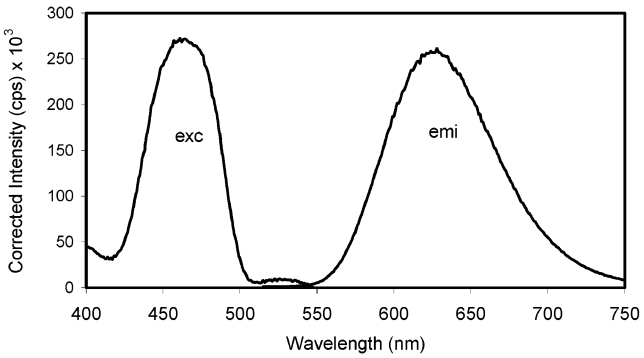

Figure 9. Excitation and emission spectra of **4** in PrCN at 77 K.

between the absorption and emission maxima; Δ) are on the order of 4500 to 5600 cm^{-1}, suggesting that the luminescence is phosphorescence. However, the nanosecond time scale is strikingly short, but not unprecedented. For example, the luminescence of **1** exhibits a τ_e of 71 $\pm$ 6 ns at 77 K.[23] On the other hand, the nanosecond time scale is too long to be assigned to a fluorescence.[42] The former assignment is preferred. The emission quantum yields appear to be constant for most species ($0.12 < \Phi_e < 0.17$), which is consistent with the similarity in τ_e data, but three of those listed in Table 6 (**5**, **6**, and **7**) exhibit 2- to 8-fold decreases. This difference remains unexplained for the moment.

(41) Plourde, F.; Gilbert, K.; Gagnon, J.; Harvey, P. D. *Organometallics* **2003**, *22*, 2862.

(42) For example, the fluorescence lifetime of the dσ*pσ singlet state of $Pt_2(POP)_4^{4-}$ ($POP^{2-} = P_2O_5^{2-}$) is 8 ps. Stiegman, A. E.; Rice, S. F.; Gray, H. B.; Miskowski, V. M. *Inorg. Chem.* **1987**, 26, 1112.

Conclusion. The investigations of **1** and **4** clearly illustrated that the structures in solution and in the solid state are not the same, which strongly suggest that **5**, **6**, **7**, and **8** must behave in the same way, and also mean that the M_n values extracted from the solution measurements do not provide information on the molecular dimension in the solid. Because of the fact that these materials are all amorphous in the solid state, their characterization becomes unquestionably more challenging. Using spectroscopic methods (UV−vis, ^{31}P NMR, FT-Raman), it was possible to demonstrate unambiguously that, despite the structural change, the $Pd_2(CNR)_4(P)_2^{2+}$ fragment remains intact in all cases. The comparison between the data extracted from the measurements of the intrinsic viscosity and T_1/NOE resulted in an important discrepancy, observed not only for this series of materials but also for a recently reported series **9** and **10**. The use of dpa instead of dppb, dpppen, and dpph and of dppp**R** instead of dppe and dppp did not greatly improve or worsen the comparison between these two techniques. The overall investigation on M_n led to the important conclusion that the T_1/NOE method has a very limited application to rigid oligomers. Finally, both series of materials ($\{Pd_2(dmb)_2(diphos)^{2+}\}_n$ and $\{Pd_2(diphos')_2(dmb)^{2+}\}_n$) exhibit reasonably intense luminescence in 77 K *n*-PrCN glasses, which contrast with most d^9-d^9 Pd_2-bonded species, but the τ_e data are unexplainably short at the moment. The strategy to use metallic fragments that are only functionalizable at the axial positions in order to synthesize polymeric or oligomeric materials is good, but this work demonstrates that ligand reorganization is possible.

Acknowledgment. This research was supported by the Natural Sciences and Engineering Research Council of Canada (NSERC).

Supporting Information Available: Table of crystal data and structure refinement, figure depicting the numbering scheme of the asymmetric unit, and tables of atomic coordinates and equivalent isotropic displacement parameters, bond lengths and angles, anisotropic displacement parameters, and hydrogen coordinates and isotropic displacement parameters for **12**. Crystallographic data in CIF format. DSC, TGA, and XRD traces for solid **1**, CPK model and MALDI-TOF data for **4**, and TGA data for **4**, **5**, **6**, **7**, **8**, and **11**. This material is available free of charge via the Internet at http://pubs.acs.org.

IC049923B